Russian Chemical Reviews **70** (4) 265 – 284 (2001) © 2001 Russian Academy of Sciences and Turpion Ltd

DOI 10.1070/RC2001v070n04ABEH000638

Size effects in chemistry of heterogeneous systems

N F Uvarov, V V Boldyrev

Contents

I.	Introduction	265
II.	Size effects in single-component systems	266
III.	Heterogeneous multicomponent solid-phase systems (composites)	271
IV.	Mechanochemical synthesis of nanocomposites and nanoparticles	278
V.	Chemical properties of nanoscale systems	280
VI.	Conclusion	282

Abstract. Size effects in single-component and multicomponent solid-phase systems are discussed. Peculiarities of the size effects in microcrystalline and nanoscale systems are analysed. Methods for mechanochemical synthesis of nanoparticles are considered. Chemical properties of nanoscale systems are analysed. Particular attention is paid to the results of studies of the properties of nanocomposites and nanoparticles. Problems concerning their stability and the possibility of mechanochemical synthesis of these systems are discussed. The bibliography includes 175 references.

I. Introduction

The understanding of basic principles and the development of new methods for the synthesis of functional materials with unusual and valuable properties is a key problem of solid state chemistry. Currently, 'dry' (*i.e.*, partially or completely solvent-free) technologies are known to be the most efficient and ecologically safe way to carry out chemical reactions.[1]

Mechanochemical processes meet this requirement. A mechanochemical reaction is a multistage process proceeding by a complex mechanism, which requires that many factors be taken into account when optimising the conditions for mechanical activation of reactants. The mechanism of a mechanochemical reaction involves the following main stages: initial deformation of the crystal structures of reactants; formation and accumulation of both point and linear defects and interaction between them; dispersion of the reactants into blocks; formation of intermediate metastable states in the regions of phase contacts and, finally, chemical homogenisation of the reaction product followed by its relaxation to reach a thermodynamically equilibrium state.

These processes have been best studied for metals where mechanochemical reactions proceed with relative ease. However, the results of recent investigations showed that ionic and molecular crystals are also promising objects for studying mechanochemical processes. In ionic crystals, the charge and potential of the double electrical layers on the phase boundaries have a pronounced effect on the interphase interaction. In molecular crystals, there is a broad spectrum of chemical bonds differing in nature, direction and energy and each type of these bonds is characterised by a specific response to mechanical treatment. By varying the type and positions of functional groups in the molecules of the crystal one can control the mechanism of mechanochemical reactions, which is of great importance for the synthesis of advanced materials.

Mechanical activation of heterogeneous mixtures allows preparation of nanocomposites with unusual properties, including supramolecular systems. Supramolecular nanoscale systems comprise chemically active components (substrates) bound to particular atoms or molecular groups of the carrier matrices (receptors) by non-covalent interactions. Such systems have been poorly studied as yet; however, a novel class of materials based on them has been designed. Unique properties of these materials are due to both specific types of intramolecular and intermolecular interactions in the bulk of the substrate and the character of the receptor – substrate interactions. Here, the role of receptor can be played by either the molecular fragments or by a particular sublattice in the crystal structure of the reactant (intercalated compounds or 'guest – host' inclusion compounds), or by active groups on the surface of heterogeneous inclusions, which favour the formation of, *e.g.*, Langmuir films or other surface layers.

A salient feature of supramolecular heterogeneous systems is the strong interface interaction, which depends on many interrelated factors including chemical, structural, morphological and thermodynamic ones. This interaction is responsible for the structural rearrangement in the substrate and for the changes in its thermodynamic, transport and chemical properties. In certain systems, the cationic or protonic conductivity of an ionic salt (substrate) can increase by several orders of magnitude and unusual phases can be stabilised in the receptor – substrate contact region. For instance, composites of the ionic salt – oxide type are candidates for the synthesis of supramolecular solid electrolytes based on them. Of considerable interest are also heterogeneous systems of the molecular crystal – oxide type.

Theoretical analysis of the mechanism of the surface interaction between different phases is a complicated problem. Currently, the properties of intergrain and phase boundaries in metals have been fairly well investigated. However, the ionic crystal – oxide or molecular crystal – oxide interfaces are still inadequately explored both experimentally and theoretically. Experimental studies are hampered by the problems of controlling the morphol-

N F Uvarov Institute of Solid State Chemistry and Mechanochemistry, Siberian Branch of the Russian Academy of Sciences, ul. Kutateladze 18, 630128 Novosibirsk, Russian Federation. Fax (7-383) 232 28 47. Tel. (7-383) 232 56 45. E-mail: uvarov@solid.nsk.su
V V Boldyrev Novosibirsk State University, ul. Pirogova 2, 630090 Novosibirsk, Russian Federation. Fax (7-383) 239 71 01. Tel. (7-383) 232 15 50

Received 20 November 2000
Uspekhi Khimii **70** (4) 307 – 329 (2001); translated by A M Raevsky

ogy of the composite, which leads to irreproducibility of the results obtained. Modern calculations require the inclusion of the contributions of not only covalent, hydrogen and van der Waals interactions but also long-range Coulomb and dipole–dipole interactions, which makes them rather difficult. Moreover, consideration of characteristic features of real interface structures is also of great importance. Nevertheless, one can carry out trial calculations of the energetically favourable surface configurations for systems of the molecular crystal (substrate)–oxide (receptor) type using the known model interaction potentials. Such estimates would be useful for targeted search of a substrate for a particular receptor.

Since the action range of surface forces is confined to a thin near-surface layer, one can expect that nanocomposites will hold the greatest promise for the synthesis of supramolecular systems. Nanocomposites are heterophasic systems, which represent dense aggregates of nanoparticles of both phases, which are uniformly distributed in the bulk. The particle size of a nanocomposite does not exceed 10 nm. In nanocomposites, virtually the whole bulk of the substrate is in the interface region, which allows experimental investigations of its physicochemical properties at the nanoscale level. To date, the properties of nanocomposites have been poorly studied, since the preparation of these systems by conventional methods is an extremely complicated task. Mechanical activation facilitates considerably the grinding of the active component and its spreading over the oxide (receptor) surface, thus favouring strong adhesive interaction.

It is known that the physical and chemical properties of solids change as the particle size decreases. These types of phenomena are usually called size effects. Numerous papers dealing with theoretical and experimental studies of size effects have appeared (see, *e.g.*, reviews [2–13]). Currently, it has been reliably shown that size effects are inherent in all solids; some phenomenological models have been proposed for qualitative or semiquantitative description of these effects.

Size effects have been best studied for metals and to a lesser degree for ionic crystals. For many materials, size effects are observed at relatively large grain size. For instance, the diffusion coefficient, conductivity and mechanical properties of a material become dependent on the average grain size (L) for $L \sim 10^3 - 10^4$ nm; as L reduces to $10 - 10^2$ nm, the melting temperature decreases and a change in the crystal lattice parameter of the material is observed. Size effect is most pronounced in nanoscale dispersed systems with a characteristic particle size in the range from 1 to 10 nm. In this case, the properties of the material can change basically, *e.g.*, it can undergo a transformation into a high-temperature phase or another high-energy state, which cannot be realised under standard conditions.

In heterogeneous systems, size effects depend on some additional factors such as the chemical nature of the components of the heterogeneous mixture, the particle morphology (spatial distribution of the components in the bulk of the composite) and the interface interaction. Consideration of these factors is a complicated problem and no satisfactory theoretical model for the description of size effects in composites has been proposed so far. The most pronounced changes in the properties are observed in both pure substances (undoped homogeneous individual compounds) and nanocomposites if the average particle size in these systems is less than 10 nm.

Recently, the interest increased in the studies of unusual effects observed in nanoscale systems. This is not surprising since the processes proceeding in such systems serve as the basis for future solid-state nanotechnologies. However, chemical reactions in solid-phase mixtures are still the least investigated aspect of solid state chemistry. This is to a great extent due to the necessity of taking into account specific features of small particles involved or formed in the reactions. For instance, the reaction system can become a nanocomposite where the properties of reactants differ substantially from those at equilibrium in the stage of nucleation of the reaction product phase. In this review, we tried to describe the most plausible mechanisms of the influence of size effects on the course of physicochemical (including mechanochemical) processes in heterogeneous solid-phase systems. In presenting the material, we pass from simple systems to more complex ones. First, size effects in isolated particles of simple substances are considered. Then, we discuss size effects in ensembles of small particles, in heterogeneous systems of different morphologies and in the nanoparticles formed in the initial stages of heterogeneous chemical reactions and prepared by mechanical activation.

II. Size effects in single-component systems

Size effects can be arbitrarily divided into two types. Weak effects where insignificant changes in the physicochemical properties of a substance are observed with an increase in the specific surface area (*i.e.*, with reduction of the particle size) belong to the first type of size effects. Here, all the changes observed can be explained by surface effects. As a rule, these effects are usually observed in crystals with a characteristic size exceeding 10 nm. These systems will be referred to as microcrystalline ones.

Strong effects where dramatic changes in the properties of a substance cannot be interpreted in terms of conventional surface phenomena belong to the second type of size effects. Most often, they are observed for very fine particles with a characteristic size of less than 10 nm. These systems will be referred to as nanoscale ones.

In this review, we will compare these two types of size effects and follow a gradual transformation of microcrystalline systems into nanoscale ones.

1. Microcrystalline systems

It has been experimentally shown that physicochemical properties of substances change noticeably as the particle size changes in the range from 10 to 100 nm. As mentioned above, the effects observed in this case are explained by the influence of the surface on the properties of crystals. As L decreases, the fraction of surface atoms increases. A 10 nm isotropic crystal of a simple substance has $\sim 1\% - 5\%$ of the atoms on the surface. The classical Gibbs thermodynamics treats all the excess thermodynamic characteristics of such fine particles, which differ from the corresponding bulk values, as being due to surface effects.

Let us consider a small particle of a substance. Ignoring adsorption, the excess Gibbs free energy, ΔG, per unit area of the tension surface is the surface tension γ of the substance. For an isotropic medium (*e.g.*, a liquid), γ equals the surface energy of the substance, σ. If the particle size (here, the diameter of a drop of the liquid) is much larger than the characteristic molecular size, the tension surface virtually matches the geometric surface of the particle. For a spherical particle, the excess energy is

$$G_s = \gamma A = \sigma A = \sigma \frac{6V}{L}, \tag{1}$$

where A, V and L are the surface area, volume and diameter of the particle, respectively. Generally, the surface tension, $\hat{\gamma}$, of a phase in an anisotropic medium is a tensor quantity. For a slightly curved surface, it is defined as the difference between the proper local value of the stress tensor, $\hat{E}$, and its bulk value, $\hat{E}_\alpha$, extrapolated to the same point and is found by integration

$$\hat{\gamma} = \int_{-\infty}^{\infty} (\hat{E} - \hat{E}_\alpha) \mathrm{d}z, \tag{2}$$

where z is the coordinate normal to the surface of the layer. The absolute value of γ is defined as half the spur (trace) of the surface tension tensor

$$\gamma = \frac{1}{2} \mathrm{Tr} \langle \hat{\gamma} \rangle = \frac{1}{2} (\gamma_{11} + \gamma_{22}). \tag{3}$$

For a liquid or an isotropic medium, $\gamma = \gamma_{11} = \gamma_{22}$ and expression (1) holds. In the crystalline phase, the surface area

can be increased in two independent ways, *viz*., by increasing the number of surface atoms and by elastic deformation of a crystal. A specific feature of a solid is the presence of an immobile structural component, the chemical potential of which is considered to be a tensor quantity.[14,15] Nonuniformity of the chemical potential distribution over the surface layer of the crystal can lead to substantial difference between the surface tension at and surface energy of different surface areas. Owing to anisotropy of the crystal lattice, each face of the crystal is characterised by its own values of the surface tension and surface energy. In addition to the crystal faces, some contribution to the excess energy of the crystal also comes from the excess energy due to the presence of edges and vertices. Assuming an ideally smooth surface, the surface tension of *i*th crystal face is related to the surface energy by the following relationship

$$\gamma_i = \sigma_i + A_i \frac{\mathrm{d}\sigma_i}{\mathrm{d}A_i}. \tag{4}$$

The effective surface energy of a crystal with N faces, M edges and Z vertices equals [16]

$$\sigma = \left(\sum_i^N \sigma_i A_i + \sum_j^M k_j l_j + \sum_k^Z \varepsilon_k \right) A^{-1}, \tag{5}$$

where k_j is the energy of formation of the jth edge, l_j is the length of the jth edge, ε_k is the energy of formation of the kth vertex (these parameters depend on the crystal shape) and $A = \sum A_i$ is the total tension surface area. The terms in formula (5) describe the contributions of crystal faces, edges and vertices to the excess energy of the crystal ignoring surface stress. For a crystal with an equilibrium shape,

$$\sigma \approx \frac{3V}{A} \frac{\sigma_i}{h_i},$$

where h_i is the distance from the Wulf point to the ith crystal face. It is appropriate to choose the parameter [16]

$$L = \frac{6V}{A} \tag{6}$$

as the characteristic crystal size.

If the parameters σ and L of a crystal are defined by formulae (5) and (6), an additional term can be entered into Eqn (1) and it can be rewritten in the form

$$G_\mathrm{s} = \gamma A = \sigma A + \Delta G_\mathrm{e} = \sigma \frac{6V}{L} + \Delta G_\mathrm{e}, \tag{7}$$

where ΔG_e is the elastic strain energy

$$\Delta G_\mathrm{e} \approx \sum A_i \frac{\mathrm{d}\sigma_i}{\mathrm{d}A_i}.$$

In real microcrystals, the ΔG_e value depends on many factors such as the crystal shape, the tension surface area A, the type of lattice symmetry, presence of defects in the crystal, *etc*. Estimation of the elastic strain energy in real crystals is a complicated problem. Expression (7) holds for both the liquid and crystalline phases (note that the contribution of elastic strain energy is nonzero only in crystals, since for liquid $\Delta G_\mathrm{e} = 0$).

As follows from the general thermodynamic expression for the Gibbs free energy,

$$G(P,T,A) = U + PV - TS + \sigma A + \Delta G_\mathrm{e}(A), \tag{8}$$

where U, V, S are the internal energy, volume and entropy of a crystal at a pressure P and temperature T, the surface area of the crystal plays the role of an additional external parameter that defines the thermodynamic properties of the material.

If the substance is highly dispersed, the contributions of the surface-dependent terms become noticeable. This leads to specific size effects such as changes in the crystal lattice parameters, low-temperature (at temperatures close to 0 K) heat capacity, the Debye temperature, phase transition temperatures and stabilisation of unusual phases. The electronic structure of the substance also changes, which is responsible for unusual optical, electrical and magnetic properties.

Among all the size effects, the effect of a decrease in the phase transition (*e.g*., melting) temperature, T_t, of small particles has been studied in most detail. Transition temperatures are determined assuming that the corresponding phases have equal Gibbs energies. In the framework of the classical Thomson model for an isolated particle, the relative change of T_t is a linear function of $1/L$ (see Refs 17–19).

$$\frac{T_\mathrm{t}}{T_\mathrm{t}^0} = 1 - \frac{6(\gamma_\alpha V_\alpha - \gamma_\beta V_\beta)}{H_\mathrm{t}} \frac{1}{L}, \tag{9}$$

where T_t^0 and H_t are the temperature and enthalpy of the phase transition from the high-temperature α-phase to the low-temperature β-phase, respectively; γ_α and γ_β are the surface tensions of the α- and β-phases at temperature T_t, respectively; and V_α and V_β are the molar volumes of the α- and β-phases, respectively. Deviation of the experimental dependences of $T_\mathrm{t}/T_\mathrm{t}^0$ on $1/L$ from linear ones can be explained by the formation of a thin film of the liquid phase on the surface of a crystal owing to melting of small particles,[20] by the dependence of γ_α and γ_β on the particle size [21] or by the contribution of elastic strain energy $\Delta G_\mathrm{e}(A)$.[11] In the last-mentioned case, Eqn (9) can be represented in the form

$$\frac{T_\mathrm{t}}{T_\mathrm{t}^0} = 1 - \frac{6(\sigma_\alpha V_\alpha - \sigma_\beta V_\beta)L^{-1} + \Delta G_\mathrm{e}(L)}{H_\mathrm{t}}, \tag{10}$$

where σ_α and σ_β are the specific surface energies of the α- and β-phases, respectively. From Eqn (10) it follows that the transition temperature depends not only on the particle size and specific surface energy, but also on the change in the molar volume, the elastic strain energy difference between two phases, $\Delta G_\mathrm{e}(L)$, and the enthalpy of the phase transition. In the case of melting, the term $\Delta G_\mathrm{e}(L)$ includes the contribution of elastic strain energy of the crystalline phase at the melting temperature.

Neglecting the ΔG_e contribution allows construction of the phase diagrams of a substance in the T–$(1/L)$ coordinates. They can be used not only for the estimation of changes in the transition temperatures, but also for the prediction of the phase size effect with a decrease in the crystal size below a certain critical value.[6,7,13] This effect manifests itself in, *e.g*., stabilisation of new phases which are atypical of the macrocrystal. Currently, numerous experimental studies have confirmed the existence of phase size effects in both films [6,7] and polycrystalline samples.[11,13] For instance, the equilibrium crystal structure of Al_2O_3 was found to be dependent on particle size. If the radius of alumina particles does not exceed 35 nm, the γ-phase is stable; if the particle size increases, γ-Al_2O_3 undergoes transformations into β-, ε-, θ- and α-Al_2O_3.[8] The formation of amorphous phases in a number of systems can also be due to size effects.[7,22,23]

In the early studies on size effects, changes in the crystal structure of small particles were explained by the effect of excess pressure,

$$\Delta p = \frac{4\gamma}{L},$$

produced owing to surface tension.[2,4] Indeed, isolated particles of many metals, alkali metal halides, oxides and nitrides exhibit a monotonic decrease in the lattice parameter with a decrease in L, which corresponds to positive Δp values. However, the unit cell parameters of nanocrystals (*e.g*., Si, Se, Cr and Pd) increase as the particle size decreases.[3] Most often, a decrease in L leads to stabilisation of high-temperature modifications rather than high-pressure phases. An explanation [24] of this fact involves the assumption of the effective negative pressure in small particles, so that the classical concept of the Laplacian pressure cannot be generally used to describe their properties.

Recently, intensive research has been carried aimed at the synthesis of highly dispersed materials such as metals, oxides, ceramics and high-melting compounds. Currently, substances with the characteristic particle size of less than 100 nm are usually classified as nanocrystalline materials.[25,26] Most of the systems studied to date are characterised by a grain size, L, ranging from 10 to 100 nm and their properties differ insignificantly from those of large crystallites. Hence, they should be considered as microcrystalline rather than nanoscale systems. As will be shown below, the systems with a particle size smaller than 10 nm can be classified as nanoscale ones. Diverse morphologies of, *e.g.*, the particles of ceramic materials complicate the problem of description of their physical properties using a unified approach. Particular effects, such as the appearance of additional contribution to the heat capacity, a decrease in the Debye temperature, an increase in the coefficients of thermal expansion and enhanced diffusion depend on the state of intergrain boundaries and can be described in the framework of an additive model which takes into account the contributions of the bulk and the surface to the physical properties of a material. In this case, the intergrain boundaries and pores in the material can be considered as specific metastable phases, the concentrations of which increase as L decreases. On the other hand, such characteristics as the magnitude of microstresses or elastic properties of the materials under study are strongly dependent on the prehistory of a sample (*viz.*, on the procedure for its preparation and heat or mechanical pretreatment). For samples with relatively large grain size, these properties can be satisfactorily described using the Hall–Petch model. As the grain size becomes less than 10 nm, the response of the dislocation structure, formed owing to the presence of intergrain boundaries, to mechanical action becomes hardly predictable;[8,12,27] however, this can also be due to inadequate experimental procedures employed in studies of these materials.

2. Nanoscale systems

Numerous experimental studies have shown that if the particle size is less than the critical size $L_c \sim 10$ nm, the bulk properties of materials change noticeably. A particle of size $L \approx 10$ nm contains $10^4 - 10^5$ atoms, of which 1% – 5% are on the surface of the particle and contribute largely to the physicochemical properties. Ensembles of such particles form nanoscale (nanocrystalline) systems in which the following characteristic effects are observed.

1. Structural changes. If $L < L_c$, the average interatomic distance in the crystal changes dramatically and the crystal lattice parameter a becomes dependent on L. In the near-surface layer, the interplanar spacings along the normal to the surface are smaller than in the bulk of the crystal,[3,4] which is due to the nonsymmetrical action of interatomic forces on the near-surface atoms. High-resolution electron microscopy (HREM) studies have shown that the region of noticeable changes in the lattice parameter is confined to five or six atomic planes and has a characteristic size $\lambda_s \sim 1-3$ nm. The same values have been obtained in calculations on alkali halide crystals.[28,29] The λ_s value can be considered as the action range of surface forces or the effective thickness of the crystal surface. The entire near-surface region of thickness λ_s is in the state that is characteristic of the surface and the crystal structure of this region depends on particular characteristics of the surface. In this connection, mention may be made that the structure of, *e.g.*, nanoscale particles of metal glasses, which is experimentally determined from the radial distribution functions, differs from the structure of the same glasses in bulk specimens.[10]

2. Changes in thermodynamic properties. In nanocrystalline systems, the Debye temperature decreases and an additional contribution to the low-temperature heat capacity of the material appears, which increases as the particle size decreases.[2,11,12,30] These effects can be explained by changes in the vibrational states of the nanocrystal,[3,4,12] namely, by 'softening' of the spectrum (an increase in the number of low-frequency modes owing to a decrease in the number of high-frequency modes) with a decrease in L. Qualitatively, 'softening' of spectra can be explained by the action of the pure surface effects: the atoms on the surface of a bulk crystal are characterised by increased amplitudes and lower vibration frequencies. However, analysis of the behaviour of the atomic Debye–Waller factors using the data of X-ray diffraction study has shown[3] that changes in the Debye temperature in nanocrystals cannot be explained only by the contribution of the vibrations of the surface atoms since a decrease in L causes a stronger lattice 'softening' than it could be expected. This means that not only the vibrational frequencies of the surface atoms, but also those of the atoms in the bulk of the nanocrystal are lowered. Yet another interesting feature of nanocrystals is that both the entropy of melting and the melting temperature decrease as L decreases.[11] Since changes in the vibrational entropy makes the major contribution to the entropy of melting, this effect is also explained by the 'softening' of the lattice of the nanocrystal with the decrease in its size.

3. Phase size effect. This is an example of a specific type of manifestation of structural and thermodynamic changes in materials. Phase size effect is most pronounced in nanoscale systems. A decrease in L down to 10–100 nm leads to stabilisation of high-temperature phases in both nanocrystals and microcrystals. In some instances, phases that are not characteristic of a given substance (including the amorphous phase) can be formed.[2,6,7,8] Structural data for even smaller particles are lacking; however, numerous theoretical studies suggest that simple substances (metals, inert gases) occur in the form of polyatomic clusters as the particle size reduces to several nanometres.[3,4,31,32]

4. Changes in the electronic properties of materials. Among the effects experimentally observed in nanoscale systems, the quantum size effect[4,7,33,34] seems to be the most interesting for chemistry. If the size of a crystal is comparable with the de Broglie wavelength of elementary excitations, the quantisation conditions of electron energy are changed and the energy bands split into a system of energy levels (Fig. 1). In semimetals, this effect leads to the appearance of low-temperature oscillations of the kinetic coefficients and optical absorption with a decrease in the thickness of specimens (films).[7] In wide-band semiconductor crystals, electronic excitation results in the formation of loosely bound electron–hole pairs. In this case, the quantum size effect manifests itself markedly as changes in the optical spectra, namely, reduction of L leads to an increase in both the energy at the maximum of the absorption band and the exciton peak intensity and to a shift of the luminescence spectrum towards the short-wavelength region. The pattern of the absorption spectrum becomes similar to that of the spectra of individual macromolecules. Semiconductor nanocrystals possessing these properties are called 'quantum dots'; they can be used in optoelectronics and are currently

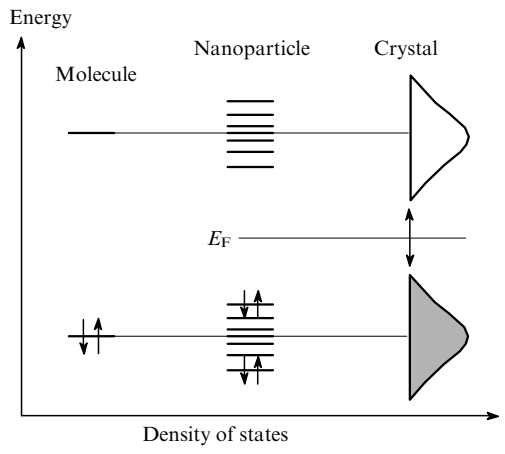


Figure 1. Electronic spectra of an isolated molecule, a nanoparticle and a semiconductor crystal. E_F is the Fermi level.

intensively studied.[33,34] As the size of ferromagnetic crystals reduces to $\sim 10-100$ nm, the coercive force increases and a decrease in the Curie temperature is observed. However, further decrease in the particle size causes a decrease in the coercive force and disappearance of ferromagnetic properties owing to the effect of superparamagnetism.[4] Ferromagnetic clusters with sizes of the order of several nanometres or layered structures with the layer thicknesses of the same order of magnitude possess abnormally high magnetoresistance coefficients.[35–37]

The above-mentioned effects can hardly be explained in the framework of the commonly accepted theory of surface phenomena. A correct mention has been made [3] that the concept of surface tension loses its meaning in the case of nanocrystals since all atoms can be treated as surface ones. Changes in the interatomic distances in small particles are mainly due to the decrease in the number of atoms in the particle,[3] which means that the size effect is a collective property of all the atoms constituting the particle. Therefore, it is helpful to follow the changes in the properties of materials on going from molecules to clusters, then to nanocrystals and, finally, to conventional bulk crystals in order to gain a deeper insight into the phenomena observed.

Let us consider pure substances with a Lennard-Jones potential of the interatomic interaction. If the number of atoms in a particle, N, is small ($N \leqslant 7$), regular polyhedral clusters are formed. If $7 < N < 13$, a large number of isomeric forms of the clusters exists, the energies of the isomers being only slightly different. If $N = 13$, a relatively stable icosahedral cluster is formed. Using this cluster as a 'seed', one can obtain larger icosahedral clusters with $N = 55$, 147, 309, 561, *etc*., by building up the atomic layers on the cluster faces.[3,4,31,32] Seldom, can large crystals of the icosahedral phase (quasicrystals) be obtained.[38,39] In addition to icosahedral clusters, pentagondodecahedral ones are also relatively stable. Owing to the presence of the five-fold symmetry axes, an increase in the cluster size should inevitably result in the development of elastic strain. According to theoretical estimates, the icosahedral and dodecahedral structures become unstable for $N \approx 500$, which corresponds to the particle size $L > \sim 2$ nm. In this case, the particle is broken into tetrahedral blocks with a close-packed, face-centred cubic (fcc) structure separated by defect domains such as systems of twin boundaries, dislocations and disclinations.[4,40] These defects provide the thermodynamic stability of the particle; in other words, small crystalline particles with imperfect structure are in the thermodynamically equilibrium state. Further increase in N leads to stabilsation of the defect-free Wulf polyhedra, the shape of which is determined from the minimum condition for the surface energy of the crystal.

Thus, each substance is characterised by two 'threshold' lengths denoted as L_1 and L_2. If the particle size of a substance is less than L_1, the particle spontaneously breaks down into nanocrystalline blocks. If $L < L_2$, a phase transition into an X-ray amorphous phase (ensemble of clusters) occurs in the particle. It should be mentioned that for small particles there is a great number of different atomic configurations with close energies.[41] This makes the concept of the equilibrium state of a particle ambiguous and is responsible for a gradual, diffuse character of phase transitions in the nanoscale systems. In particular, melting of clusters is considered as a dynamic equilibrium between the 'solidlike' and 'liquidlike' clusters that coexist at any temperature.[41,42]

On going from individual clusters to ensemble of nanoparticles, the effect of intergrain boundaries on the physicochemical properties of the ensemble becomes noticeable. Since the number of surface atoms in a nanoparticle is comparable with that in the bulk, in the case of random packing of particles the structure of each crystallite is 'tuned' to correspond to the local environment, which leads to effective broadening of the intergrain boundaries. Information on the structure of intergrain boundaries in nanoscale materials is contradictory. Both strongly disordered boundaries with a loose amorphous structure [9,10] and the boundaries with relatively high concentration of atoms (typical of bulk polycrystals) are observed.[12] In a 10 nm nanocrystal with an intergrain boundary width of 0.5–1 nm, the fraction of the atoms situated on these boundaries reaches 15%–30% of the total number of atoms.[10,12] Depending on the conditions for the preparation and annealing of ceramic nanoparticles, the structures of the intergrain boundaries can be different. Freshly prepared specimens have more disordered structures compared to either sintered or simply stored specimens in which the boundary atoms are ordered to form conventional intergrain boundaries. This is accompanied by the growth of crystallites owing to a decrease in the concentration of disordered boundary atoms. According to molecular dynamics calculations of model ensembles using the Coulomb or Lennard-Jones interatomic potentials,[43,44] these relaxation processes should be observed after intense mechanical deformation of nanoscale systems.

3. Transport properties of microcrystals and nanocrystals

Polycrystalline materials are characterised by increased mobility of atoms. This has been confirmed in studies on the kinetics of sintering and recrystallisation,[45] diffusion of radioactive isotopes [46] and ionic conductivity.[47,48] In bulk crystals, diffusion and mass transfer occur by migration of point defects which has an activation character. Earlier, enhanced diffusion in fine crystallites was thought to be due to changes in the concentration of vacancies caused by curvature of the crystallite surface. In fact, the expression for the excess concentration of point defects in a metal near the curved surface, $[V_M]$, obtained using the Thomson–Kelvin equation for the equilibrium of vacancies in crystal, has the form [45]

$$[V_M] = [V_M]_\infty \exp\left(-\frac{2\gamma\upsilon}{RkT}\right) = [V_M]_\infty \exp\left(-\frac{Q}{kT}\right), \qquad (11)$$

where $[V_M]_\infty$ is the concentration of defects in the bulk and R is the radius of curvature. If $\gamma = 100$ erg cm^{-2} and $\upsilon = 10$ cm^3 mol^{-1}, the curvature of the surface makes an additional contribution, Q, of 0.003 eV ($R = 10$ nm) and 0.03 eV ($R = 1$ nm) to the energy of formation of defects. This effect can lead to a noticeable increase in the concentration of defects only in very fine particles with the size of about 1 nm.

Currently, it is accepted that the activation energy of grain boundary diffusion in metals is lower than that of bulk diffusion; this is explained by the relatively loose local grain boundary structure and by high concentration of boundary defects.[10,46] The formation of a defect in the bulk of a metal involves two stages,[49] namely, the formation of a pair comprising an excess atom above the surface and a vacancy in the surface layer and detachment of the vacancy from the surface followed by its diffusion into the interior of the metal. This is illustrated in Fig. 2 in which the plots of changes in the free energy of the crystal upon the formation of a surface vacancy and its diffusion into the bulk of the metal are also presented. In the first stage, surface disordering occurs: the metal atom M goes out of the surface layer on the outer surface of the crystal, which leads to the formation of a pair of defects, *viz*., the adatom, M_s, and a vacancy in the surface layer, V_{Ms}. The concentration of defects on the surface, $[V_{Ms}]$, and in the bulk, $[V_M]_\infty$, are determined by the corresponding energies of formation (g_s and g_0, respectively)

$$[V_{Ms}] = [M_s] = \exp\left(-\frac{g_s}{2kT}\right), \qquad (12)$$

$$[V_M]_\infty = \exp\left(-\frac{g_0}{kT}\right). \qquad (13)$$

Surface diffusion can occur owing to both migration of atoms over the outer surface and migration of vacancies within the surface layer. In polycrystals, the role of the outer surface is played

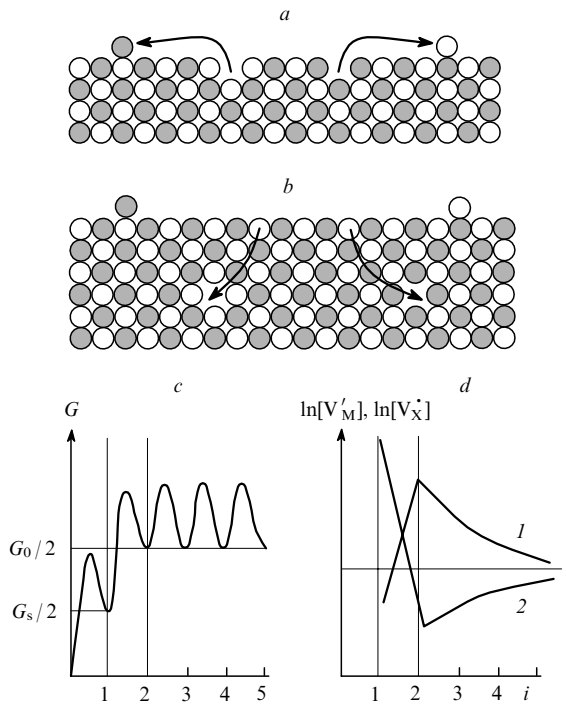


Figure 2. Schematic representation of the elementary act of surface disordering (*a*) and the formation of a Schottky defect in the bulk of a crystal (*b*) as well as change in the Gibbs free energy of the crystal upon the formation of a defect (*c*) and the spatial distribution of defects in the near-surface layer of the ionic crystal of the MX type (*d*).
$[V'_M]$ is the concentration of cationic vacancies (*1*), $[V^{\bullet}_X]$ is the concentration of anionic vacancies (*2*); *i* is the order number of the near-surface layer along the normal to the surface directed into the interior of the crystal ($i = 1$ corresponds to the outer surface of the crystal).

by the intergrain boundaries; in this case, $[M_s] \approx 1$ and surface disordering is described by the equation

$$[V_{Ms}] = \exp\left(-\frac{g_s}{kT}\right). \tag{14}$$

The energy of formation of a defect and, hence, the concentration of defects in the bulk of the crystal are determined by the fundamental properties of matter rather than surface disordering. On the contrary, the g_s value can vary between 0 and g_0 depending of many factors such as orientation of the surface, the type of intergrain boundary, adsorption of impurities on the surface, *etc*.[50] Hence, the activation energy of surface diffusion should depend on the procedure for the preparation of a given material.

In ionic crystals of the MX type, surface disordering is accompanied by the formation of the electrical double layer since both cationic (V'_{Ms}) and anionic ($V^{\bullet}_{Xs}$) vacancies within the surface layer can be formed independently in accordance with the equations of quasichemical reactions

$$0 \rightleftarrows V'_{Ms} + M^{\bullet}_s, \tag{15}$$

$$0 \rightleftarrows V^{\bullet}_{Xs} + X'_s \tag{16}$$

(here, zero corresponds to a perfect crystal).

As in the case of metals, the concentration of uncharged surface defects should be completely determined by the energy of formation of these defects

$$g_s = (g_{V_M})_s + (g_{V_X})_s.$$

However,

$$(g_{V_M})_s \neq (g_{V_X})_s,$$

hence, an excess surface charge and the corresponding surface potential φ_s appear. The magnitude of φ_s depends on the energy difference between the quasichemical surface disordering reactions:[50]

$$\varphi_s = \frac{(g_{V_X})_s - (g_{V_M})_s}{2e}. \tag{17}$$

The concentration of the Schottky defects in the bulk of a crystal is determined by the equilibrium constant of a quasichemical reaction involving the formation energy of bulk defects of g_0,

$$0 \rightleftarrows V'_{M\infty} + V^{\bullet}_{X\infty}. \tag{18}$$

The concentrations of defects on the surface,

$$[V'_{Ms}] = [V'_{M\infty}] \exp\left(\frac{g_0 - g_s}{2kT} + \frac{e\varphi_s}{kT}\right), \tag{19}$$

$$[V^{\bullet}_{Xs}] = [V^{\bullet}_{X\infty}] \exp\left(\frac{g_0 - g_s}{2kT} - \frac{e\varphi_s}{kT}\right) \tag{20}$$

depend on both the surface potential (17) and the additional contribution of the surface disordering. In the absence of the latter, (*i.e*., in a particular case $g_0 = g_s$), Eqns (19) and (20) coincide with the expressions obtained in the framework of Frenkel's model.[51, 52] Analogous expressions can also be obtained for crystals with Frenkel defects.

The parameter φ_s can be considered as the potential jump at the crystal–vacuum interface; this takes into account the properties of the surface, in particular, specific adsorption of charged particles (vacancies) on the surface. The defects localised on the surface can form a dense diffusion layer. At low concentrations of defects, the properties of this layer (or the space charge region) are described in the framework of the Gouy–Chapman model. The concentration of defects in the diffusion layer is calculated using the Poisson–Boltzmann equation which relates the space charge to the potential. The simplified expression for the ionic conductivity due to the electrical double layer has the form [53]

$$\varkappa = \frac{B}{L} T^{-1/2} \exp\left[\left(-\frac{h_0}{4} + \frac{e\varphi_s}{2} - E_m\right)(kT)^{-1}\right], \tag{21}$$

where B is the constant which includes all temperature-independent terms, h_0 is the enthalpy of formation of the defect, E_m is the migration energy of the defects that form the electrical double layer; for simplicity, the entropy contribution to φ_s is taken as zero. The expression for the conductivity of the diffusion layer written in the coordinates of the Arrhenius equation has the form:

$$\log(\varkappa T^{1/2}) = \log\frac{B}{L} - \frac{E_a}{kT},$$

where the activation energy of conductivity is

$$E_a = \frac{h_0}{4} - \frac{e\varphi_s}{2} + E_m.$$

Two regions corresponding to the high-temperature and low-temperature conductivities can be seen on the plot of experimental temperature dependence of the conductivity of a polycrystalline ionic salt. The former corresponds to the intrinsic conductivity, while the latter is due to the contribution of surface defects and is described by Eqn (21).

The mobility and transport properties of atoms in small crystals or in clusters have not been studied so far. Nevertheless, computer simulation predicts high mobilities of the atoms and points out that a distinctive feature of the mechanism of migration is its collective character.[3, 54] This has been confirmed by the results of experimental studies of nanocrystalline powders of pure substances.[55–57] For instance, the coefficient of self-diffusion in

copper nanocrystals at 271 K is 14 to 20 orders of magnitude greater than in conventional bulk copper.[55] An analogous effect was also found in studies of bulk diffusion in nickel nanocrystals.[56]

However, one should treat the interpretation of the results obtained in studies of self-diffusion with caution. A critical analysis [58] of the experimental results obtained in a study of diffusion in Cu, TiO_2 and Pd nanocrystals [57] has shown that correct consideration of the diffusion 'suction' into the bulk of the crystal makes the coefficient of surface diffusion in Cu nanocrystals typical of polycrystalline copper rather than abnormally high. It has also been mentioned [58] that the coefficients of oxygen diffusion in TiO_2 nanocrystals are 5–6 orders of magnitude greater than in bulk crystals and that the coefficients of diffusion of the dissolved hydrogen in palladium nanocrystals are greater than in the bulk specimen.

III. Heterogeneous multicomponent solid-phase systems (composites)

Generally, a solid-phase composite is a complex, heterogeneous multicomponent system which comprises several real solid phases considered as components. By a real solid phase is meant a totality of single crystals of different sizes, which contain impurities, point lattice defects, dislocations and pores as well as free surfaces (*e.g.*, cracks, intergrain and outer boundaries). Many properties of composites depend on their morphologies, namely, the particle size distribution of each phase and mutual spatial arrangement of monophasic domains. From the standpoint of connectivity of their components, composites can be divided into (i) three-dimensional random mixtures of different phases, (ii) layered and (iii) columnar structures.[59, 60] Film and porous structures can also be considered as composites. Real heterogeneous systems are usually characterised by mixed morphologies.

When studying composites, one should take into account both the properties of each individual phase and those of interphase boundaries. If different phases interact with one another, the interfaces can exhibit specific properties that are characteristic of neither of the individual phases. It is appropriate to use the thermodynamic approach to describe the properties of heterogeneous systems and find the conditions for their stability. We will restrict ourselves to consideration of two possible types of the surface interaction (a weak interaction and a strong one) between components of a simple system taking a two-phase composite as an example.

1. Interface interaction and sintering of composite

For a two-phase composite composed of macrocrystalline phases (phase 1 and phase 2) with weak interaction between them, the Gibbs energy, G, can be thought to be approximately equal to the sum of the Gibbs energies of the pure components:

$$G = G_1 + G_2 .$$

In real polycrystalline specimens, the energies G_1 and G_2 depend not only on the bulk parameters but also on a number of additional factors such as the presence of (i) dislocations and corresponding elastic strain, (ii) point defects, (iii) interfaces and outer surfaces, *etc*. Assuming that the largest contribution to the total excess Gibbs energy of the real pure components comes from their surface energies, one can write:

$$G = G_1 + G_2 + G_s = (G_1^\circ + G_2^\circ) + (G_{s1} + G_{s2}). \qquad (22)$$

Here, G_1° and G_2° are the standard Gibbs energies and G_{s1} and G_{s2} are the surface energies of the components, which are defined for each component by expression (7).

Long-term heat treatment of such a composite leads to conventional sintering accompanied by growth of crystallites of both phases and annealing of dislocations.[45] After sintering, the Gibbs energy of each phase becomes close to its bulk value, G_1° and G_2°, and the system reaches a thermodynamic equilibrium. If the mixture was mechanically treated in such a manner that the particle sizes of one or both components decreased substantially, a post-annealing phase separation will occur in the composite to give a mixture of the initial macrocrystalline phases (Fig. 3 *a*).

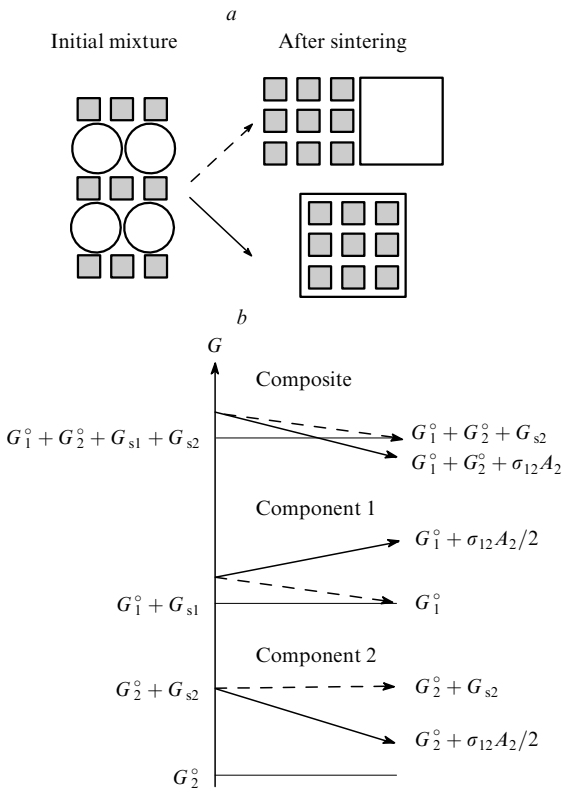


Figure 3. Schemes of sintering (*a*) and changes in the Gibbs energy of a composite (*b*) in the absence of adhesion between the components (dashed arrows) and in the case of strong adhesion (solid arrows).

Let us consider the case where the rates of recrystallisation and annealing of the component 1 are much higher than those of the component 2. The expression for the Gibbs energy of the composite annealed at the sintering temperature of the component 1 can be written in the form

$$G = G_1^\circ + G_2^\circ + \sigma_2 A_2 + \Delta G_{e2} . \qquad (23)$$

After sintering, the component 1 reaches an equilibrium state ($G_1 = G_1^\circ$), though the entire system remains thermodynamically nonequilibrium since the component 2 remains dispersed. Changes in the Gibbs energy of the composite are schematically shown in Fig. 3 *b*.

If surface interaction occurs between the constituent phases of the composite, an additional term, G_{s12}, appears in the expression for the Gibbs energy; this term represents the total change in the Gibbs energy of a heterogeneous system owing to the appearance of interphase contacts

$$G = G_1 + G_2 + G_{s12}. \qquad (24)$$

The G_{s12} is calculated as follows

$$G_{s12} = \sigma_{12} A_{12} ,$$

where σ_{12} is the specific surface energy of the interface and A_{12} is the interface area between the components 1 and 2. The contribution of the elastic strain energy should be taken into account by introducing additional terms, ΔG_{e1} and ΔG_{e2}. The total Gibbs energy of the composite with inclusion of surface interaction is

$$G = (G_1^\circ + \sigma_1 A_1 + \Delta G_{e1}) + (G_2^\circ + \sigma_2 A_2 + \Delta G_{e2}) + \sigma_{12} A_{12} . \qquad (25)$$

The expression for the Gibbs energy of the component 2 of the composite can be obtained from Eqn (25)

$$G_2 = G_2^\circ + \sigma_2 A_2 + \sigma_{12}\frac{A_{12}}{2} + \Delta G_{e2}, \quad (26)$$

assuming that the interface energy is evenly distributed between the components 1 and 2. The contribution of the elastic strain energy, ΔG_{e2}, to the total energy of the phase 2 is mainly determined by the elastic strain energy due to the crystal lattice misfit at the phase 1 – phase 2 interface and by the energy of misfit dislocations formed in the near-interface regions.[6–8] Calculations of G_e values are very complicated even for simple thin film morphology, which make estimation of this contribution in composites difficult. Nevertheless, irrespective of the character of elastic strain (a dilation or compression strain), the contribution ΔG_{e2} is always positive and should increase with an increase in A_{12}. Thus, the third and fourth terms in expression (26), which determine the energy of the phase 2, depend on the interface area in the composite.

Sintering of a mixture of a low-melting component 1 with the greater self-diffusion coefficient with nanoparticles of a high-melting compound 2 can lead to both a decrease and an increase in the interface area A_{12}. In the former case, sintering results in conventional recrystallisation of the phases. In the latter case, which is of particular interest for solid state chemistry, the formation of the interface is thermodynamically favourable if

$$\frac{dG}{dA_{12}} < 0.$$

Sintering is accompanied by an increase in the interface area A_{12}. Neglecting the dependences of the specific surface energies and elastic strain energy on the surface area (or particle size) and expressing σ_{12} in terms of the free energy of adhesion (σ_a),

$$\sigma_{12} = \sigma_1 + \sigma_2 - \sigma_a,$$

one can write

$$\frac{dG}{dA_{12}} = \sigma_1\frac{dA_1}{dA_{12}} + \sigma_2\frac{dA_2}{dA_{12}} + \sigma_1 + \sigma_2 - \sigma_a. \quad (27)$$

The formation and growth of the interface (the so-called 'sticking') have been considered in detail.[45,61,62] The mechanism and kinetics of 'sticking' are different in two cases defined by the conditions

$$\sigma_a < 2\sigma_1, \quad (28)$$

$$\sigma_a > 2\sigma_1. \quad (29)$$

If condition (28) is met, a 'neck' is formed between two particles of the composite. The shape and size of the 'neck' depend on the shapes and sizes of the particles and on σ_1, σ_2 and σ_a. Inequality (29) is known as the Gibbs – Smith condition for ideal wetting of films. If this condition is met, phase 1 completely covers the particle of the phase 2 after sintering.

Inequalities (28) and (29) also determine the growth mechanism of the films of the phase 1 on a support formed by the phase 2. Growth of island films according to the Volmer – Weber mechanism is observed in the former case while a steady layer-by-layer growth of films according to the Franck – van der Merve mechanism is observed in the latter case.[6,63] The inequality (29) follows from expression (27) if

$$\frac{dG}{dA_{12}} < 0, \quad \frac{dA_1}{dA_{12}} \approx 1, \quad \frac{dA_2}{dA_{12}} = -1,$$

i.e. if a decrease in the free surface area of the component 2 (the support) leads to the formation of an equivalent free surface area of the component 1 (the film). Considering the general case of an arbitrary morphology of the initial mixture of the components 1 and 2, one can see that the newly formed free surfaces of the component 1 can overlap if the distance between the surfaces of the phase 2 is sufficiently short (see Fig. 3 *b*). Complete overlap of these free surfaces makes the derivative dA_1/dA_{12} close to zero and, assuming that the following conditions are met,

$$\frac{dG}{dA_{12}} < 0, \quad \frac{dA_1}{dA_{12}} = 0, \quad \frac{dA_2}{dA_{12}} \approx -1$$

from Eqn (27) it follows that

$$\sigma_a > \sigma_1. \quad (30)$$

This inequality determines the condition for spreading of the component 1 over the surfaces of the phase 2 in the composite. Comparison of inequalities (30) and (29) (the condition for ideal wetting or epitaxy in films) shows that the surface interaction in composites must be much stronger and requires a lower adhesion energy than in conventional film structures. It is known that roughness of a surface improves its wetting and that the roughness factor can vary between 0 and 1. Inequality (30) corresponds to the limiting case where the coefficient of roughness of the surface of the phase 2 is equal to unity.

If condition (29) or (30) is met, a spontaneous increase in the interface area or 'wetting' of the well-developed surface of the component 2 with the component 1 occurs in the system. If compound 2 is in the nanocrystalline state, the effective particle size of the phase 1 can be substantially reduced. In other words, an unusual effect, *viz.*, self-dispersion of the component 1 to give a two-phase nanocomposite, will be observed. Self-dispersion is an indicator of a strong interface interaction in the system. This interaction will occur during the long-term sintering of the composite until the entire surface of the component 2 will be covered with the component 1. In this limiting case, $A_{12} \approx A_2$ and the system reaches the state of metastable equilibrium, where

$$G = (G_1^\circ + G_2^\circ) + \sigma_{12} A_2 + (\Delta G_{e1} + \Delta G_{e2}), \quad (31)$$

$$G_1 = G_1^\circ + \sigma_{12}\frac{A_2}{2} + \Delta G_{e1}(A_2). \quad (32)$$

The effect of self-dispersion was experimentally observed in, *e.g.*, solid-phase sintering of composites $AgCl - Al_2O_3$ (see Ref. 64), $AgI - Al_2O_3$ (see Ref. 65) and $Li_2SO_4 - Al_2O_3$ (see Ref. 66). An analogous effect was detected in the heterogeneous systems based on alkali nitrates and halides such as $LiNO_3 - Al_2O_3$ and $NaNO_3 - Al_2O_3$ (see Ref. 67), $RbNO_3 - Al_2O_3$ and $CsNO_3 - Al_2O_3$ (see Ref. 68), $NaCl - Al_2O_3$, $KCl - Al_2O_3$ and $RbCl - Al_2O_3$ (see Ref. 53). This is indicative of strong adhesion of ionic salts to the alumina surface.

Analysis of expression (32) shows that the properties of an ionic salt depend not only on the standard thermodynamic parameters of the material, but also on the contribution of the energy of interface interaction, which increases as the oxide surface area increases. If the components are taken in a 50 : 50 (vol.%) ratio and mixed uniformly and an ideal wetting of the entire surface of the oxide with the MX component is achieved, the effective MX grain size is nearly equal to half the particle size of the oxide. In the composites with nanoscale oxide particles ($\sim$10 nm), the size of the MX particles becomes sufficiently small to provide noticeable size effects.

2. Adhesion energy and formation of point defects at the interface

Stable interphase contacts require that the energy of adhesion be sufficiently high. Generally, the mechanism of adhesion depends on the character and strength of the interaction between the atoms arranged on the contacting surfaces. The authors of classical monographs on adhesion [69–71] have studied the systems in which the major contribution to the surface interaction comes from the dispersion forces. In this case, the energy of adhesion can be calculated using the Hamaker – de Buhr theory

$$\sigma_a = 2(\sigma_{d1}\sigma_{d2})^{1/2} + \sigma'_{12}, \quad (33)$$

where σ_{d1} and σ_{d2} are the contributions of the dispersion forces to the surface energies of the components 1 and 2, respectively, and the last term includes the contributions of the non-dispersion interactions, *viz*., the ion–ion, donor–acceptor, dipole–dipole interaction, *etc*. In composites of the ionic salt–oxide type, it is the last term of expression (33) that makes the largest contribution to the energy of adhesion. In the absence of the electrical double layers, the σ_a value can be approximately estimated using the model of 'weak boundary layers',[72] according to which the work of adhesion is equal to the geometric mean of the works of cohesion of the components

$$\sigma_a \approx (W_1 W_2)^{1/2} = 2(\sigma_1 \sigma_2)^{1/2}. \quad (34)$$

From relationships (34), (29) and (30) it follows that self-dispersion should occur if $\sigma_2 > \sigma_1$ and be enhanced with a decrease in σ_1. Among alkali halides, lithium salts are characterised by the highest specific surface energies σ, while cesium salts are characterised by the lowest ones, the σ values being monotonically decreased on going from fluorides to iodides.[29] Therefore, self-dispersion should proceed most easily in the composites based on cesium iodide and have the lowest rate in the systems based on lithium fluoride. However, it was noted [70] that the model of 'weak boundary layers' [72] does not take into consideration specific characteristics of the interface in composites (its morphology and the presence of surface-active centres), which prevents a correct separation of the contributions of different types of interactions to the surface energies of the components, and does not assume the formation of the double surface layers.[72] Therefore, this model allows only qualitative estimation. To carry out more reliable calculations, one should take into account the structure of the contact surface and the potentials of the ion–ion interactions at the ionic crystal–oxide interface, which represents an extremely complicated problem that has not been solved so far. Approximate estimates of the surface energy using the Harkins 'broken bond' method have shown [13, 69, 73] that σ increases in proportion to the crystal lattice energy for isostructural compounds, the coefficient of proportionality being dependent on the type of the corresponding crystallographic plane. Comparison of the σ values for alkali halides [29] with the corresponding values for oxides Al_2O_3, FeO, MgO and SiO_2 (100–300 and 600–1200 erg cm^{-2}, respectively) [13, 69] shows that the wetting condition (30) should be met for the composites based on ionic halides and high-melting oxides including alumina.

Physically, a tendency of the components of composites of the ionic salt–oxide type to decrease the surface energy owing to the ion–ion interaction at the interface is the reason for rerrangement of surface layers. To a first approximation, the MX–A interface energy (MX is the ionic salt and A = Al_2O_3)

$$G^s_{MX-A} = \sigma_{MX-A} A_{MX-A} \approx \approx E_{M-Al} + E_{Al-X} + E_{M-O} + E_{X-O} \quad (35)$$

is determined by the sum of the energies of the cation–cation ($M^+ - Al^{3+}$), cation–anion ($Al^{3+} - X^-$ and $M^+ - O^{2-}$) and anion–anion ($X^- - O^{2-}$) interactions. For the sake of simplicity, let us assume that strong interfacial interaction provides a structural correspondence between the crystal lattices of the MX and A phases. Since the energies E_{M-Al}, E_{X-Al}, E_{M-O} and E_{X-O} differ from one another, an ideal structure of the boundary layer of each phase will be distorted to provide an additional gain in the surface energy owing to the mutual approach (or removal) of different surface ions. The magnitudes of the displacements of the ions from ideal positions are determined by the balance of energies E_i. Since the sizes of the anions of alumina and most of MX salts are larger than those of the cations, one can expect that, provided that both contacting phases are close-packed, the cations at the interface are displaced to longer distances than anions. As a result, an intermediate, positively charged layer enriched with cations is formed between the surface layers of the components (Fig. 4) and

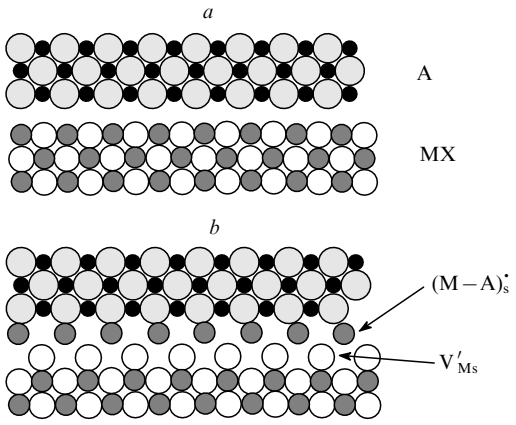


Figure 4. A scheme for the formation of defects at the interface between two binary ionic compounds.
Initial surfaces (*a*) and interface (*b*).

a layer of cationic vacancies (V'_{Ms}). Such a structural relaxation can be represented as the following quasichemical reactions:

$$0 \rightleftarrows V'_{Ms} + (M-A)_s^{\bullet}, \quad (36)$$

$$0 \rightleftarrows V'''_{Al} + (Al-MX)_s^{\bullet\bullet\bullet}, \quad (37)$$

which describe the surface disordering in MX (36) and Al_2O_3 (37) at the MX–A interface. In addition to reaction (36), interstitial cations also can be transferred into the space charge layer [48, 74]

$$M_i^{\bullet} \rightleftarrows (M-A)_s^{\bullet}. \quad (38)$$

The formation of surface defects at the MX–A interface can also proceed by other mechanisms. If the energy of the interaction between aluminum cations and X anions is sufficiently high, the following reactions can proceed at the interface:[75]

$$0 \rightleftarrows V_X^{\bullet} + (X-A)'_s, \quad (39)$$

$$0 \rightleftarrows M_i^{\bullet} + (X-A)'_s. \quad (40)$$

Reaction (39) is analogous to reaction (36) except that the role of cations is played by the anions; this can occur in composites based on fluorides, *e.g*., PbF_2–A (A = CeO_2, ZrO_2, SiO_2, Al_2O_3).[75] Reaction (40) can be observed in $AgF-Al_2O_3$ composites. Since the binding energy of Al–X dramatically decreases on going from fluoride anions to other halide anions, the reactions (39) and (40) in $MX-Al_2O_3$ systems are unlikely. More probable is the reaction

$$0 \rightleftarrows X'_i + (M-A)_s^{\bullet}, \quad (41)$$

which can occur in the salt-based MF_2-SrCl_2 composites with the anti-Frenkel defects.

Shukla *et al*.[75] proposed to use the pE value of the isoelectric point of an oxide as an indicator of the surface activity of the oxide. Indeed, equations analogous to Eqns (36) and (39) can also be written for the surface interaction of an oxide with water

$$H_2O \rightleftarrows OH' + (H-A)_s^{\bullet}, \quad (42)$$

$$2H_2O \rightleftarrows H_3O^{\bullet} + (OH-A)'_s, \quad (43)$$

The former reaction dominates for oxides with p$E > 7$ (*e.g*., Al_2O_3, CeO_2) and the latter is predominant for oxides with p$E < 7$ (ZrO_2, SiO_2). By analogy with aqueous solutions one can expect that the surface reactions (36), (38) and (41) are typical of composites with basic oxides (p$E > 7$), while reactions (39) and (40) are typical of acid oxides (p$E < 7$). Currently, the lack of experimental data makes it impossible to assess the transferability of the model of acid-base equilibria in aqueous solutions to

composites. Nevertheless, the competition between the processes (36) and (42)

$$V'_M + (M-A)^{\bullet}_s + H_2O \rightleftarrows OH' + (H-A)^{\bullet}_s + M^*_M , \qquad (44)$$

where M^*_M is a cation with a zero effective charge, can be responsible for deterioration of the ionic conductivity of the composites $AgCl-Al_2O_3$ (see Ref. 64) and $AgI-Al_2O_3$ (see Ref. 65) and for the appearance of protonic conductivity in the composites $Li_2SO_4-Al_2O_3$ (see Ref. 76) and $M(NO_3)_n-Al_2O_3$ (see Refs 77 and 78) in a humid atmosphere.

3. Ionic conductivity of composites

In essence, reactions (36)–(41) represent the formation of an electrical double layer at the $MX-Al_2O_3$ interface. The formation of this layer affects the properties of the oxide; *e.g.*, a decrease in the Néel temperature of iron(III) oxide was observed in $AgI-Fe_2O_3$ composites.[79] The effect of the electrical double layer on the properties of the ionic salt is even more pronounced. A change in the energy upon the displacement of the ion from its normal (equilibrium) position characteristic of isolated MX crystal to the space charge layer (Δg_{i-A}) can be considered as the work of charging of the surface; therefore, Δg_{i-A} is related to the surface potential at the MX–A interface

$$\varphi_{As} \sim \frac{\Delta g_{i-A}}{q_i} , \qquad (45)$$

where q_i is the charge of the displaced ion. The exact φ_{As} value is determined not only by the Δg_{i-A} value, but also by the contribution of the spatial relaxation of the oxide ions; therefore, relationship (45) should be considered only as a correlation between Δg_{i-A} and φ_{As}. If adhesive binding is strong, the Δg_{i-A} value is always negative; hence

$$\varphi_{As} > 0 \text{ for } q_i < 0$$

and

$$\varphi_{As} < 0 \text{ for } q_i > 0.$$

For $T = 0$, there is a dense layer on the surface of the MX particle contacting the oxide. This layer is analogous to the Helmholtz layer. An increase in temperature leads to the formation of a diffusion space charge layer built of cationic vacancies, which is responsible for enhanced conductivity of the composite since the ion mobility in the dense layer is low. The mobilities of defects in the diffusion layer are taken to be equal to their mobilities in the bulk of the crystal[48,74] since the concentration of defects in this layer is low and the crystal structure remains unchanged (no deformations, surface phase transitions, *etc.*). In this case, the conductivity of the composite is given by expression (21) with φ_{As} introduced instead of φ_s and the migration energy E_m corresponding to those defects which form the diffusion layer; for the sake of simplicity, the entropy contribution to φ_{As} is taken as zero. For low potential φ_{As}, which corresponds to a relatively weak surface interaction, the conductivity is low and the activation energy of conductivity is

$$E_a = \frac{h_0}{4} - \frac{e\varphi_{As}}{2} + E_m .$$

Here, E_a ranges from $h_0/4 + E_m - e\varphi_{As}/2$ to $h_0/4 + E_m$ and depends on the state of the MX–A interface (on the presence of structural defects, adsorbed impurities, *etc.*). Therefore, the conductivity parameters measured in the experiments are poorly reproducible, which is sometimes observed in poorly sintered composites.

If the surface potential φ_{As} is high, the energy of adhesion is rather high, which favours the formation of a dense interphase contact and a substantial increase in the charge density in the diffusion layer. As φ_{As} increases, the concentration of surface defects increases and at a surface potential equal to

$$\varphi_{As} = \frac{h_0}{2e} , \qquad (46)$$

a full coverage of the surface with the similarly charged ions or defects is attained. If $e\varphi_{As} > h_0/2$, several layers of similarly charged ions should be on the surface, which is unlikely. Thus, the condition (46) determines the maximum value of the surface potential $e\varphi_{As}$ in a composite.[53] In composites with high surface potential, the concentration of surface defects is close to the limiting value. In this case, the conductivity and activation energy of conductivity are given by the relationships

$$\varkappa = \frac{A}{L} T^{-1/2} \exp\left(-\frac{E_m}{kT}\right),$$
$$E_a = E_m . \qquad (47)$$

The results obtained using these expressions are in good agreement with the experimental data for composite systems $AgCl-Al_2O_3$, $AgBr-Al_2O_3$, $TlCl-Al_2O_3$ and $LiI-Al_2O_3$.[48]

Certain new factors affecting the transport properties of ionic salts appear on going to nanoscale systems. The assumption of constant mobilities of defects within the diffusion layer and in the bulk of the crystal is acceptable if the thickness of the space charge region, $2\lambda_D$, does not exceed the size of the MX crystal. It is reasonable to assume that the mobilities of defects within the diffusion layer of the crystal depend on the position of the defect owing to the drag effect of the ion 'atmosphere'. Near the MX–A interface, the defect mobility is low; it gradually increases with distance from the surface and reaches a maximum deep in the interior of the crystal. Size reduction of the MX crystal (this can be achieved by increasing the concentration of A) leads to a decrease in the defect mobilities and to an increase in the activation energy of conductivity, which is equal to the migration energy of the defect. This effect is noticeable if the crystal size L is less than $2\lambda_D$. In fact, the activation energy of conductivity in $AgI-Al_2O_3$ nanocomposites monotonically increases as the oxide concentration increases.[65]

If $L < \lambda_D$, the total concentration of defects in the bulk of the crystal becomes high. The defect–defect interactions in crystals can lead to phase transitions into the superionic state.[80–82] It cannot be ruled out that the superionic phases can be formed in the near-surface region of the crystal. The formation of the superionic phase on the surface of the pure ionic crystal has been reported;[83] in composites, this seems to be even more probable.

If the concentration of defects, n, is temperature-independent, the expression for conductivity has the form

$$\varkappa = n\left(\frac{e^2 a^2 v_0}{6kT}\right)\exp\left(\frac{S_m}{k}\right)\exp\left(-\frac{E_m}{kT}\right), \qquad (48)$$

where a is the jump length of the defect, v_0 is the vibrational frequency of the mobile ion and S_m is the entropy of migration, which can be calculated using the formula for the compensation effect

$$S_m = \frac{E_m}{T^*} ,$$

observed in alkali halide crystals. In this case, $T^* = 2.1 \times 10^3$ K.[84] The formula given below[85] relates the conductivity of the composite at 25 °C to the activation energy of conductivity and to the concentration of defects in the MX particles; it includes the compensation effect and uses two empirical parameters, $a = 0.3$ nm and $v_0 = 3 \times 10^{-12}$ s^{-1}, typical of ionic crystals,

$$\log \varkappa_{25}\,(\text{S cm}^{-1}) = \log n\,(\text{cm}^{-3}) - 14.5\,E_a\,(\text{eV}) - 20.55. \qquad (49)$$

Figure 5 presents the experimental data for different composites. The straight lines were plotted using Eqn (49) with different defect concentrations. The experimental data for a number of superionic conductors are also shown in Fig. 5. As can be seen, the

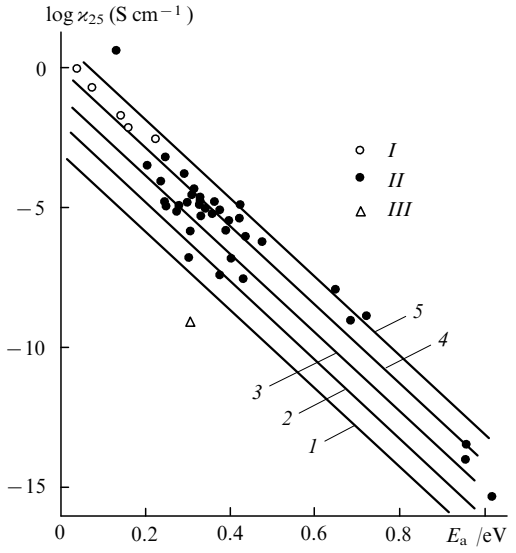


Figure 5. Theoretical (straight lines) and experimental (points) dependences of the conductivity of superionic conductors (*I*), composites (*II*) and AgCl single crystal (*III*) at 25 °C on the activation energy for conductivity at different concentrations of defects: 10^{17} (*1*), 10^{18} (*2*), 10^{19} (*3*), 10^{21} (*4*) and 10^{22} cm^{-3} (*5*).[85]

concentration of defects in the composites with the highest conductivity is also high and close to the corresponding values for superionic conductors. This indicates the possibility of stabilisation of disordered phases in composites.

4. Size effects in heterophasic systems

In studies of thin films it has been shown that the structures of solids in the near-interface regions depend strongly on peculiarities of the morphology and energetics of the contacting planes. As a rule, the epitaxial interphase contact is the most energetically favourable. In the case of strong adhesive binding, building up the layer of phase 2 on a support proceeds by the van der Merve mechanism. Owing to the crystal lattice misfit between the adjacent phases, elastic strain is accumulated in the bulk of the component 2 (the elastic strain energy increases as the thickness of the layer of phase 2 increases).[6, 86, 87] According to calculations,[88] the continuous layer is destroyed after reaching a certain critical thickness h_c and a network of misfit dislocations is formed at the interface. If the lattice misfit parameter lies between 0.1% and 1%, the calculated thickness of the epitaxial layer, h_c, is $\sim 5-25$ nm (see Ref. 88), which is consistent with the experimental data. If the rate of film precipitation is high, thin films with an amorphous structure are deposited on the support instead of the epitaxial layer. As the temperature or the thickness of the layer increases, the amorphous phase undergoes transformation into a crystalline film.[7] The formation of thin epitaxial or amorphous films can be considered as manifestation of the phase size effect in heterogeneous systems, *viz*., the reduction of the characteristic size (film thickness) leads to the formation of new surface phases.

In composites, the role of the thickness of the epitaxial layer is played by the average distance between the grains of the inert component 2 (r_{22}). At low concentrations of the phase 2, the distance between the grains of this phase exceeds h_c and the properties of the phase 1 are similar to those of the island thick films oriented parallel to the faces that confine the intergrain space. On the contrary, at high concentrations of the component 2, the phase 1 is distributed in the micropores of the phase 2 after sintering. In this case, if the grain size of the phase 2 is sufficiently small (less than 10 nm), one gets $r_{22} < h_c$ and the phase 1 occurs in the form of a thin layer or a surface phase. Since the properties of substances in the surface phase differ substantially from the bulk properties of the same substance, two phases can coexist in composites, *viz*, the surface phase with anomalous properties and a conventional bulk polycrystalline phase with a high concentration of dislocations.

Thermodynamic properties of substances coated on solid supports in the form of adsorbed layers or thin films differ from their bulk properties.[2–7, 18, 19, 89] Noticeable distinctions between the thermodynamic properties appear at a characteristic crystal size of ~ 10 nm.[2–7] Changes in the temperatures of phase transitions that occur in the bulk of the component 1 can be estimated using the formula

$$\frac{T_t}{T_t^0} = 1 - \left(\sigma_{\alpha 1}A_{\alpha 1} + \sigma_{\beta 1}A_{\beta 1} + \frac{\sigma_{\alpha 12}A_{\alpha 12} - \sigma_{\beta 12}A_{\beta 12}}{2} + \Delta G_e\right)H_t^{-1}, \quad (50)$$

where the subscripts α and β correspond to the α- and β-phases at temperature T_t, respectively, and ΔG_e is the excess elastic strain energy difference between these phases. If the changes in the volume and ΔG_e upon the phase transition are small ($A_{\alpha 1} \approx A_{\beta 1} \sim L^{-1}$; $A_{\alpha 12} \sim A_{\beta 12} \sim L^{-1}$; $\Delta G_e \approx 0$), the temperature of the phase transition into the α-phase decreases, which is usually observed in thin films. Some examples of the phase diagrams constructed in the coordinates $T_t - (T, L^{-1})$ for different supported metal films are available in the literature (see Refs 6–8, 18, 19). According to these phase diagrams, transition temperatures can decrease by hundreds of degrees upon reduction of L to 10 nm.[6, 7] Generally, the temperatures of phase transitions in composites can either decrease or increase depending on the particular form of the functions $G^\circ = f(T)$, $\sigma = f(T)$ and $\Delta G_e = f(T)$ for a given component in different phases.

The results of studies on the physicochemical properties of composites $AgI-Al_2O_3$ (see Refs 65, 90–94), $Li_2SO_4-Al_2O_3$ (see Ref. 66), $LiNO_3-Al_2O_3$, $NaNO_3-Al_2O_3$, $KNO_3-Al_2O_3$ (see Ref. 67), $RbNO_3-Al_2O_3$ (see Refs 68 and 95), $CsNO_3-Al_2O_3$ (see Ref. 68), $CsHSO_4-SiO_2$ (see Refs 96 and 97), $CsCl-Al_2O_3$ (see Ref. 98) with the specific surface area of Al_2O_3 particles, s, of 270 m^2 g^{-1} show that nanocomposites prepared by self-dispersion technique exhibit unusual structural, thermodynamic and transport properties. Thermodynamic calculations for all the above-mentioned systems showed that bulk chemical interaction at the temperatures of synthesis of nanocomposites is thermodynamically unfavourable. This is also confirmed by the results of special experiments on the sintering of the initial mixtures under 'severe' conditions (high temperatures and long-term heat treatment).

Thermodynamic properties of silver iodide in $(1-x)AgI-xAl_2O_3$ nanocomposites differ substantially from those of pure AgI. This can be illustrated by nearly complete absence of the thermal effect at 147 °C upon the phase transition into the α-phase of AgI in the nanocomposite with high Al_2O_3 concentrations ($x > 0.8$). Presumably, the superionic α-phase is stabilised in the composite; however, the absence of AgI reflections in the X-ray diffraction patterns (including those typical of the α-phase) suggests that silver iodide is in the amorphous state. This is also confirmed by the absence of a thermal effect at the melting transition in AgI (see Ref. 93) and by the unusual luminescence spectra observed upon UV irradiation of the nanocomposite.[94] More detailed studies have shown that an increase in the Al_2O_3 content in the composite leads to a gradual change in the properties of silver iodide. Namely, two phase transitions are observed instead of one $\alpha \rightarrow \beta$ transition, which gradually disappear as x increases. Both transitions are characterised by distinct hysteresis loops on the plots of the temperature dependences of conductivity and heat capacity, the temperature of the high-temperature phase transition depends slightly on x, while the temperature of the low-temperature phase transition decreases appreciably as the mole fraction of Al_2O_3 increases (see Refs 92 and 93).

This suggests that silver iodide can occur in two crystalline states during sintering of the composites under study. These are

the bulk state with the properties of pure AgI and the surface state localised at the $AgI-Al_2O_3$ interface. The properties of the latter are affected by the interfacial interaction. Like the bulk state, the surface crystalline state can be in the high-temperature and low-temperature disordered phases. As the Al_2O_3 content increases, the effective intercrystallite distance in the oxide (and the effective particle size of AgI) decreases and the conductivities of both phases approach each other, thus indicating a gradual levelling of distinctions between the phases.

In addition to this effect, the increase in the concentration of Al_2O_3 leads to a dramatic decrease in the enthalpies of melting and $\beta \rightarrow \alpha$ phase transition in AgI, which points to the appearance of the interface amorphous AgI phase in the composites (Fig. 6). At sufficiently high concentration of alumina, nearly all the silver iodide can be stabilised in the interface amorphous state.[91, 93, 94] It was shown that doping of AgI with Al_2O_3 leads to a decrease in the temperature and enthalpy of the phase transition in AgI.[99, 100] This is in excellent agreement with the results of our investigations of composites with low Al_2O_3 content. However, the authors of the papers cited (*cf.* Refs 99 and 100) have observed only minor changes in the transition temperature and enthalpy, since the heterogeneous additive used in their experiments was a relatively coarse-grained (0.06 μm) Al_2O_3. The use of alumina with a grain size of 0.01 μm allowed us to observe much more pronounced effects.

Composites $MNO_3-Al_2O_3$ (M is an alkali metal) (see Refs 67, 68, 95) and the $CsHSO_4-SiO_2$ system[96, 97] behave analogously. DTA studies of composites $(1-x)RbNO_3-xAl_2O_3$ have shown[95] that all the phase transition temperatures of $RbNO_3$ including the melting temperature remain virtually unchanged upon sintering, whereas the enthalpies of the phase transitions decrease dramatically. For $x \geqslant 0.7$, the DTA curves exhibit no peaks indicating the presence of crystalline $RbNO_3$ in the composite (Fig. 7). Instead, a weak broad peak appears near 250 °C with the maximum intensity for $0.4 < x < 0.6$.

These effects are not observed in the composites containing coarse-grained Al_2O_3 (with grain sizes of several micrometres),

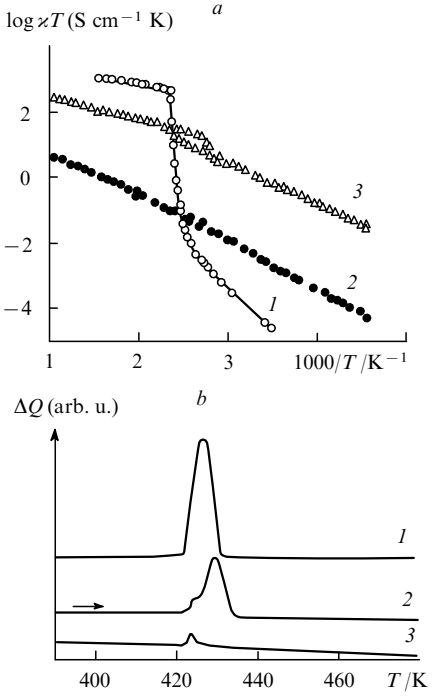


Figure 6. Temperature dependences of conductivity (*a*) and DTA curves (*b*) for pure AgI and the $(1-x)AgI-xAl_2O_3$ composites.[93]
AgI (*1*), $x = 0.6$ (*2*), $x = 0.8$ (*3*).

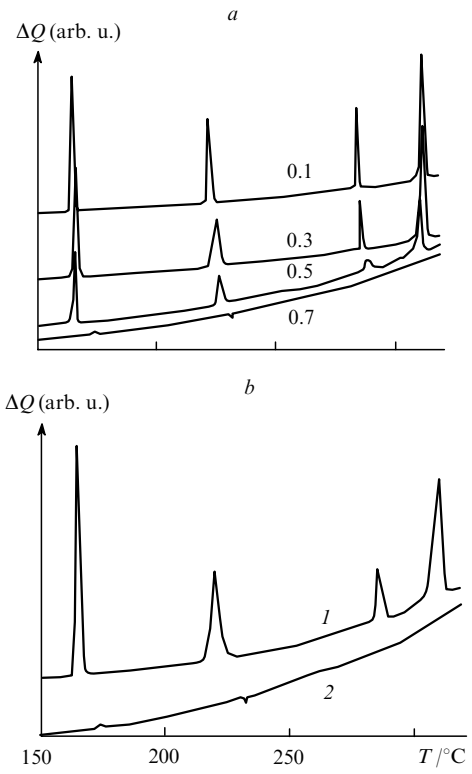


Figure 7. DTA curves for the $(1-x)RbNO_3-xAl_2O_3$ composites with a specific surface area of 270 $m^2\ g^{-1}$ (*a*) and for the $0.7\ RbNO_3-0.3\ Al_2O_3$ composites (*b*) with a specific surface area of 10 (*1*) and 270 $m^2\ g^{-1}$ (*2*). Figures near the curves shown in Fig. 7 *a* represent *x* values.[95]

which means that they are due to the influence of the oxide grain surface. Electron diffraction studies and conductivity measurements revealed the formation of an amorphous phase of $RbNO_3$ in the $RbNO_3-Al_2O_3$ composites. The thermal effect at 250 °C is due to the glass transition in the amorphous phase and the transition temperature is much higher than the calculated value (−55 °C).[101] However, it should be taken into account that in this case the amorphous $RbNO_3$ phase is formed at the $RbNO_3-Al_2O_3$ interface and its properties can be very different from those of pure amorphous rubidium nitrate. The results of thermodynamic studies of $RbNO_3-Al_2O_3$ composites are consistent with those obtained by the ionic conductivity measurements, Raman spectroscopy and X-ray diffraction analysis.[95]

The concentration and thickness of the interface phase in composites can be estimated using a simple brick-wall model for cubic particles.[85, 93, 95] The model is based on the assumption that the brick size is equal to the particle size of the dispersed additive (L_A) and uses the following formulae for the calculation of the volume fraction, f_s, or the mole fraction, x_s, of the interface phase

$$f_s = \beta \frac{2\lambda}{L_A} f(1-f), \tag{51}$$

$$x_s = \beta \frac{2\lambda}{L_A} \frac{\gamma x(1-x)}{1+x(\gamma-1)}, \tag{52}$$

where β is the geometric factor, λ is the thickness of the surface layer, f and x are the volume fraction and molar concentration of the dispersed phase 2 (the oxide A), respectively, and the coefficient γ depends on the densities (d) and molecular masses (μ) of the components and is defined as follows

$$\gamma = \frac{\mu_A d_1}{\mu_1 d_A}.$$

The fraction of the ionic salt (f_1 or x_1) that remained in the bulk phase can be calculated using the expressions

$$f_1 = 1 - f - f_s = \left(1 - f\beta\frac{2\lambda}{L_A}\right)(1 - f), \quad (53)$$

$$x_1 = 1 - x - x_s = 1 - x - \beta\frac{2\lambda}{L_A}\frac{\gamma x(1-x)}{1 + x(\gamma - 1)}. \quad (54)$$

These formulae are convenient for estimating the thickness of the interface phase provided that the particle size of the dispersed component, L_A, is known. The ratio λ/L_A and the thickness of the interface phase, λ, can be estimated from the concentration dependence of any extensive characteristic of the phase 1 in the composite using expressions (53) or (54) (Fig. 8). According to calculations, the amorphous layer in $AgI-Al_2O_3$ and $RbNO_3-Al_2O_3$ composites is respectively 3 [93] and 4 nm [95] thick.

Studies of the conductivity of the nitrate-based composites revealed a substantial increase in the low-temperature conductivities and disappearance of the conductivity jumps observed upon phase transitions. Note that the Arrhenius plots of the temperature dependences of conductivity are nonlinear (Fig. 9). Among the composites based on alkali nitrates, the greatest increase in conductivity is observed for the $LiNO_3$-based ones. At 100 °C, the conductivity of the composite $0.5\,LiNO_3-0.5\,Al_2O_3$ is 7 orders of magnitude higher than that of pure lithium nitrate.[67] The smallest increase in conductivity is observed for the $CsNO_3-Al_2O_3$ system.[68] Similar effects were also found in $CsHSO_4-SiO_2$ composites.[96,97] Here, the physicochemical characteristics of cesium hydrosulfate depend on the pore size of silica gel used as a dispersed additive, that is, there is an optimum pore size ($\sim$2 nm) at which the thermodynamic, structural and transport properties of $CsHSO_4$ change to the greatest extent.[97]

Physicochemical properties of lithium sulfate change substantially on going from the bulk crystal to $(1-x)Li_2SO_4-xAl_2O_3$ nanocomposites.[66,85] The low-temperature ionic conductivity of the composite substantially increases while the well-defined (for pure Li_2SO_4) phase transition becomes diffuse in the composite (Fig. 10). The results of DTA studies of these composites showed that lithium sulfate occurs in two states at low oxide concentrations. One state exhibits the properties of the initial Li_2SO_4 while the other state possesses the properties of the phase localised near the $Li_2SO_4-\gamma$-Al_2O_3 interface. If the content of Al_2O_3 additive, x, exceeds 0.5, virtually the whole lithium sulfate is stabilised in the interface phase after sintering. In composites with the oxide particle size of the order of several nanometres the concentration of the interface phase is very low and no additional thermal effect is observed. Compared to the pure substance, the phase transition in the interface phase of Li_2SO_4 occurs at a much lower temperature (470 °C).

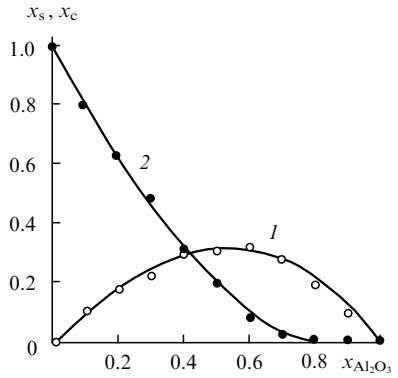


Figure 8. Dependences of the mole fraction of the interface amorphous phase (x_s) (curve *1*) and crystalline phase (x_c) (curve *2*) of AgI on the Al_2O_3 content in the $AgI-Al_2O_3$ composites according to DSC measurements of the enthalpy of the $\alpha-\beta$ phase transition in AgI. Solid lines represent the results of calculations with $\lambda \approx 4$ nm and $L_A \approx 10$ nm.[93]

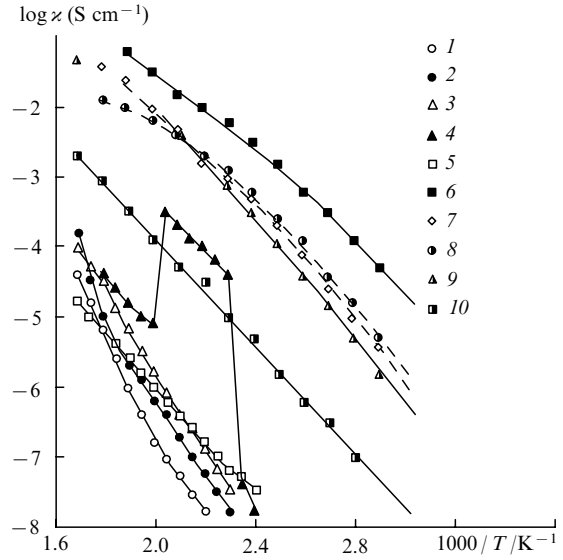


Figure 9. Temperature dependences of conductivities of nitrates MNO_3 (*1–5*) and composites $0.5MNO_3-0.5Al_2O_3$ (*6–10*); M = Li (*1*, *6*), Na (*2*, *7*), K (*3*, *8*), Rb (*4*, *9*) and Cs (*5*, *10*).[67,68]

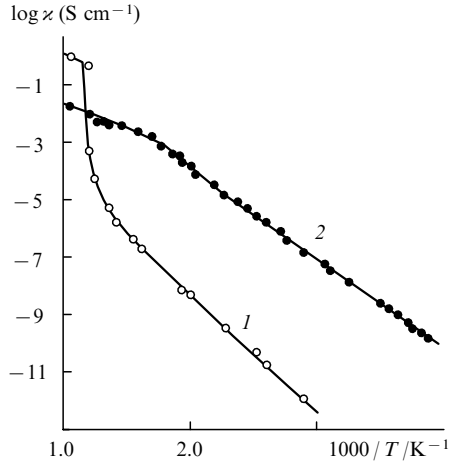


Figure 10. Temperature dependences of the ionic conductivities of pure Li_2SO_4 (*1*) and the $(1-x)Li_2SO_4-xAl_2O_3$ nanocomposite (*2*).[66]

In this case, the mechanism of adhesion involves a stage of surface chemical reaction between Li_2SO_4 and Al_2O_3 resulting in the formation of a thin interface lithium aluminate layer. The thickness of this layer was estimated at 1–2 monolayers on the surface of the Al_2O_3 grains. Analysis of the X-ray and electron diffraction patterns of the nanocomposite points to epitaxial character of the lithium sulfate layers, which is due to the close (111) interplanar spacing in Li_2SO_4 and Al_2O_3 and to strong adhesion of Li_2SO_4 to the alumina surface. Lithium aluminate forms an intermediate layer and represents a specific 'glue', which provides a denser epitaxial contact between the Li_2SO_4 and Al_2O_3 nanocrystals.

The nanocomposite $0.33\,Li_2SO_4-0.67\,Al_2O_3$ can be prepared in two ways, *viz.*, by sintering of the starting materials and by decomposition of the precursor, $Li_2SO_4 \cdot 4\,Al(OH)_3 \cdot mH_2O$.[85] The second method allows one to synthesise a nanocomposite with uniform distribution of the components and an average particle size of less than 10 nm for both Li_2SO_4 and Al_2O_3 (Fig. 11). If the alumina particles are uniform in size, both synthetic procedures

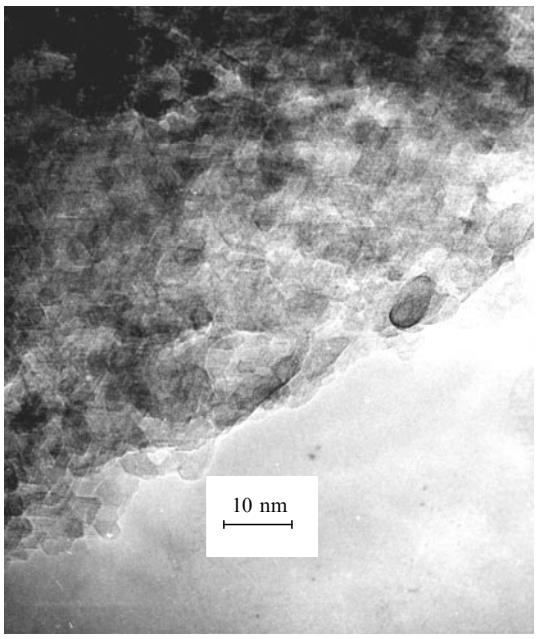


Figure 11. Morphology of the $Li_2SO_4-Al_2O_3$ nanocomposite obtained by thermal decomposition of its precursor, $Li_2SO_4 \cdot 2Al(OH)_3 \cdot mH_2O$.[66]

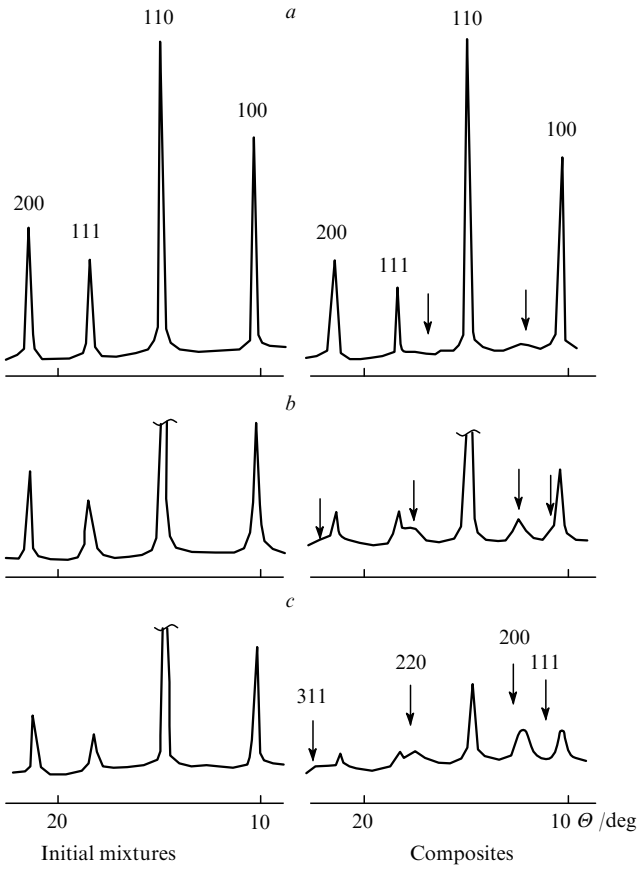


Figure 12. X-Ray diffraction patterns of the initial mixtures and $(1-x)CsCl-xAl_2O_3$ composites after long-term sintering at 600 °C. Arrows denote the reflections corresponding to the fcc phase of CsCl, figures denote the crystallographic plane indices.
$x = 0.3$ (*a*), 0.6 (*b*), 0.8 (*c*).

result in the formation of nanocomposites with identical structural, transport and thermodynamic characteristics after sufficiently long-term heat treatment of the mixtures. This indicates that the composites reached metastable thermodynamic equilibrium. Decomposition of precursors, $Li_nX \cdot 2nAl(OH)_3 \cdot mH_2O$, allows the preparation of nanocomposites with different lithium salts Li_nX (X = F, Cl, Br, I, SO_4, PO_4); these systems exhibit high ionic conductivities.[85]

X-Ray diffraction and DTA studies of $(1-x)CsCl-xAl_2O_3$ composites (with Al_2O_3 with a specific surface area, σ, of 270 $m^2\ g^{-1}$) showed that long-term sintering leads to stabilisation of a high-temperature CsCl phase localised at the interface (Fig. 12).[53,98] No changes are observed in the X-ray diffraction patterns as the particle size of Al_2O_3 increased up to ~ 1 μm; this is in agreement with the known results.[102] The size effect, *i.e.*, stabilisation of the high-temperature CsCl phase, seems to be due to the interface interaction, which is most pronounced in the composites with nanocrystalline additives.

In the ionic salt – Al_2O_3 systems, lithium salts form nanocomposites somewhat more easily than rubidium and cesium salts and iodides form nanocomposites more easily than chlorides or fluorides. This points to important role of the polarising power of the cation and the polarisability of the anion in the mechanism of surface interaction.

IV. Mechanochemical synthesis of nanocomposites and nanoparticles

Mechanochemical processes proceed at low temperatures where the formation of a perfect crystal structure is difficult. Therefore, the use of mechanochemistry for the synthesis of metastable products, in particular, nanoparticles and nanocomposites, is of considerable interest.[103–109] Mechanochemical methods for the preparation of nanocrystalline materials have been intensively developed recently [105–108] and investigations into the fundamental problems associated with the formation, relaxation and stabilisation of metastable states during mechanical activation seem to be of great importance.

1. Mechanical action on a solid and the formation of nanoscale systems

Mechanical action leads to the development of elastic stress in the crystal. For different reasons (crystal lattice anisotropy, specific features of electronic and ionic properties, different energies of chemical bonds), elastic stress relaxation can follow different mechanisms such as vibrational and electronic excitations, ionisation of chemical bonds, bond cleavage, rearrangements of atoms and migration of atoms and ions.[109] By varying the intensity and character of mechanical action one can control the properties of materials obtained by mechanical activation.[104]

One of the most often encountered effects accompanying mechanical activation is failure which leads to grinding of the particles of a substance. Failure is preceded by accumulation, interaction and concentration of defects as well as by crack formation and propagation into the interior of the crystal. However, direct mechanical grinding of a solid usually does not allow preparation of nanoparticles since mechanical activation leads to acceleration of mass transfer owing to the formation of metastable defects. In addition, the stored elastic strain energy is partly transformed into thermal energy and the temperature in the impact zone can be significantly increased, thus favouring both recrystallisation of the substance and 'healing' of defects that prevent grinding.[106]

Mechanical activation of heterogeneous mixtures seems to be more promising for the preparation of nanoparticles. Initially, the harder component acts as a crusher, thus favouring finer grinding of the softer component. Dispersion in deeper activation stages is due to the interfacial interaction between the components; here, the soft component plays the role of surfactant and facilitates the grinding of the harder component owing to the Rehbinder effect.

Mechanochemical reactions in heterogeneous mixtures represent the most efficient method for the preparation of nanocomposites.[106–108] In this case, nanoparticles of a new phase are

formed at the interface or as a result of decomposition of metastable states stabilised upon mechanical activation of the mixture. A unique feature of mechanochemical processes is the possibility of 'deformation mixing' (mechanical alloying) of the components of a mixture, *i.e.*, mixing of the starting components at the atomic level.[105–109] Mechanical alloying occurs at low temperatures whereupon diffusion is retarded. This allows stabilisation of various metastable intermediates including nanoparticles.

2. Methods for mechanochemical synthesis of nanocomposites and nanoparticles

Mechanochemical synthesis of nanocomposites in metal systems is fairly well studied. The main classes of mechanochemical reactions used for the preparation of metal nanocomposites are as follows.[110]

1. Conventional mechanical treatment of a composite resulting in transformation of one of the components into the nanocrystalline state.

This is the simplest and most widely used procedure for the preparation of nanocomposites by exposing mixtures of solids to high-power mechanical impulses. If one component of a mixture is hard while the other is soft, mechanical treatment will lead to comminution of the former and deformation of particles of the latter. This can result in the formation of a composite comprising plate-like particles of the soft component with a thickness of several nanometres separated by large nanoparticles of the hard component.

This type of nanocomposites has been obtained in, *e.g.*, bimetallic systems Cr–Fe,[111] Ni–Ti[112] and Ce–Yb[113] (for a detailed list of systems, see the review by Matteazzi *et al.*[114]). Mechanically alloyed $Cu_{30}Cr_{170}$ has been obtained by treatment of a Cu–Cr mixture[115] and studied by EXAFS, DSC and anomalous scattering of synchrotron radiation. It was shown that the alloy represents a nanocomposite rather than a solid solution of copper in chromium and that the Cu nanoparticles occur in the metastable phase. Mechanical treatment of a Cu–Co mixture, 80 : 20 (at.%), allowed the preparation of a nanocomposite containing nanoscale cobalt particles.[116] Thorough field-ion microscopy studies of the structure of the nanocomposite showed that the material contains both individual 15-nm Co nanoparticles and 1–3-nm cluster inclusions of Co atoms in the copper matrix.[117] The presence of small Co clusters is responsible for anomalous magnetoresistance of the nanocomposite. Layered Co–Cu structures obtained by vapour deposition or using pulse electrochemical deposition also possess analogous properties.[118]

2. Transformation of an amorphous phase into a nanocrystal owing to the elastic strain energy stored during mechanical treatment, *e.g.*, preparation of nanocomposites from amorphous alloys based on iron and aluminium:[119]

$$A_aB_b \text{ (amorphous solid)} \longrightarrow A_aB_b \text{ (nanocrystal)}.$$

Yet another example is the transformation of amorphous Fe–Si–B alloys into nanocrystals upon mechanical treatment. The process can be either accelerated by addition of cobalt or slowed down by addition of niobium (this can inhibit crystallisation and retain the amorphous alloy). The reasons for the transformation of the amorphous phase into a crystalline one upon mechanical treatment have been discussed.[120–122] If mechanical treatment is carried out in air, the formation of nanocomposite is often favoured by the formation of an oxide film on the metal surface.[119]

3. Decomposition of an amorphous phase (usually, an intermetallide) to give one of the components in the form of nanoparticles:

$$A_aB_b \text{ (amorphous solid)} \longrightarrow c\,A \text{ (nanocrystal)} + A_{a-c}B_b \text{ (amorphous solid)}.$$

4. More complex mechanochemical reactions:

$$a\,A + b\,B \longrightarrow A_aB_b \text{ (nanocrystals)},$$

$$A_aB_b + C \longrightarrow A_aB_bC \text{ (nanocrystals)},$$

$$A_aB_b + C_cD_d \longrightarrow A_aB_bC_cD_d \text{ (nanocrystals)}.$$

Mechanical alloying of the mixtures of different metals with graphite, silicon or tin is used for the preparation of carbide,[114, 123] silicide and stannide nanoparticles.[124] Nanocomposites can also be obtained by mechanochemical solid-phase displacement and exchange reactions, *e.g.*, by the interaction of iron nitride with aluminium or silicon or by the reaction of iron carbide with chromium[125]:

$$Fe_{2.5}N + Al \longrightarrow AlN \text{ (nanocrystals)} + 2.5\,Fe,$$

$$4\,Fe_{2.5}N + 3\,Si \longrightarrow Si_3N_4 \text{ (nanocrystals)} + 10\,Fe,$$

$$Fe_3C + 3\,Cr \longrightarrow (Fe,Cr)_3C \text{ (nanocrystals)}.$$

Hydrogenation of an intermetallide $Pr(Co_{1-x}Cu_x)_5$ results in the formation of copper and cobalt nanoparticles with sizes 10–20 nm incorporated into the matrix of hydrogenation products $Pr(Co_{1-y}Cu_y)_5H_x$ and PrH_2 (see Ref. 126).

Specific methods are used if one needs to obtain nanoparticles of a single component of a nanocomposite rather than the nanocomposite itself. For instance, nickel–zinc ferrite nanoparticles with sizes 8–50 nm were obtained by long-term (200 h) heat treatment of a mixture of the ferrite and quartz.[127] To separate the metals from quartz and other components, the mixture was treated with 2 M $HClO_4$ for 1 h. This kind of treatment makes the particles on the ferrite surface charged, whereas other particles remain uncharged; this phenomenon is used for the separation of the mixture. Ferrite particles form a sol that can be destroyed by controlled change in the pH.

An efficient method for preparation and isolation of nanoparticles from mechanically alloyed composites has been proposed recently.[128–130] Nanoparticles were formed by solid-phase exchange reactions chosen in such a way that the by-products be readily soluble while the desired product, *i.e.*, nanoparticles, be insoluble in conventional solvents. For instance, ZnS nanoparticles were prepared by the solid-phase mechanochemical reaction

$$ZnCl_2 + CaS \longrightarrow ZnS + CaCl_2.$$

The newly formed zinc sulfide particles with an average size of 500 nm were found to represent aggregates comprised of smaller particles with characteristic sizes of 10–12 nm. The formation of aggregates can be prevented by adding calcium chloride to the initial mixture; in this case, the desired product is obtained as separated ZnS particles of size 7–9 nm. Calcium chloride is removed from the mixture of reaction products by selective dissolution in methanol followed by centrifugation. A similar procedure is used for the synthesis of CdS nanoparticles following the reaction

$$CdCl_2 + Na_2S \longrightarrow CdS + 2\,NaCl.$$

The starting mixture was additionally diluted with NaCl. After mechanical treatment for 1 h the mixture was washed with water to remove NaCl. The sizes of the CdS particles formed were from 4 to 8 nm (*i.e.*, less than the Bohr radius of an exciton), which allowed the mechanochemical synthesis of 'quantum dots'.

Mechanochemical reduction of oxides is also known. The use of a peroxide instead of oxide allows transformation of this reaction into self-propagating high-temperature synthesis.[131] By performing the reaction in the 'smouldering' (incomplete combustion) rather than conventional combustion regime (this can be achieved by changing the heat treatment regime of the mixture or by diluting it with an inert compound), one can obtain the reaction product in the form of nanoparticles with sizes 40–50 nm. Using this regime in the reactions of BaO_2 with metals, mixed titanium-molybdenum oxide, barium aluminate and barium stannate nanoparticles were obtained.[131]

Preparation of zinc ferrite nanoparticles by mechanical treatment of a mixture of zinc and iron oxides represents yet another example of mechanochemical synthesis of nanoparticles of complex oxides from simple ones. However, in this case heating leads to rapid growth of stable large ferrite crystals.[132] Mechanical treatment of the preliminarily prepared zinc ferrite, α-Fe_2O_3 and γ-Al_2O_3 nanoparticles also leads to their growth.[133] Therefore, optimisation of reaction conditions (in particular, mechanical treatment) should receive due attention when performing mechanochemical synthesis of nanoscale materials.

A specific case of mechanical activation of a topochemical reaction has been studied.[134] Intercalation of γ-$Al(OH)_3$ (gibbsite) with lithium salts from solution was shown to result in the development of wedging stress in the gibbsite lattice. This leads to an increase in the interlayer distances in the gibbsite structure, thus improving the intercalation conditions. Relaxation of mechanical stress can lead to the appearance of lattice defects. This will also favour an enhancement of the reactivity of gibbsite and can be used for carrying out various chemical reactions in the interlayer space of gibbsite.[135–138]

A salient feature of this type of reactions is the possibility of crystallographic control of mutual orientation of the reactants, intermolecular distances and their mobilities. Nanoparticles can be prepared by intercalating the reactants into the interlayer space. They can be formed either if both reactants are present within the interlayer space or if the second reactant (*e.g.*, oxygen) is supplied from the outside to oxidise the first reactant in the interlayer space. Nanoparticles thus formed can sometimes be retained within the interlayer space, as is the case of $[MnO_x(OH)_4]^{4-2x-y}$ nanoparticles formed by the reaction of the intercalated permanganate ions and unsaturated organic acids.[139] In other cases, the products can form a separate phase and break down the layered matrix structure, as in the thermal decomposition of complexes intercalated into the structure of hydrargillite (monoclinic gibbsite).[140]

V. Chemical properties of nanoscale systems

In studies of nanoparticles and heterogeneous nanoscale systems it is of great importance to take into account a 'feedback' between the reactivities of solid reactants and the character of the reaction between them.[1]

There are different forms of such a 'feedback'. Sometimes, it can arise owing to the development of mechanical stress due to the absence of structural correspondence between the starting substances and the reaction product (the so-called misfit).[141,142] In other cases, the reaction product can affect the electron–hole equilibrium or the concentration of ionic defects in the region adjacent to the starting point of the reaction. Finally, the 'feedback' can manifest itself in transformation of a kinetically controlled reaction into a diffusion-controlled one if the molecular volume of the product is larger than the molecular volumes of the starting materials. It should also be kept in mind that the 'feedback' can depend on the particle size of the solid reactants and products.

1. Properties of particles formed in the initial stages of heterogeneous chemical reactions

Let us consider the oxidation of lower iron and manganese oxides as an example. Here, the size effect can manifest itself in the dependence of the composition of the reaction products on the sizes of their particles. In some instances, the mechanism of a solid-phase reaction can change upon change in the particle sizes of the reactants. This is thought to be due to transformation of a homogeneous system into a heterogeneous one, as is the case of, *e.g.*, oxidation of Fe_3O_4 into Fe_2O_3.[143,144] Oxidation of fine Fe_3O_4 particles with a size less than 300 nm is a homogeneous process which involves the formation of a solid solution of oxygen in the magnetite lattice accompanied by gradual transformation of the Fe_3O_4 crystal lattice into the γ-Fe_2O_3 lattice. Oxidation of larger Fe_3O_4 particles is a heterogeneous process since the Fe ions have no time to diffuse through the whole bulk of the particle, so it is only the surface layer that is oxidised. The appearance of the oxide concentration gradients and the development of stress in the surface layer of the particles facilitate the nucleation of rhombohedral Fe_2O_3. Analogously, fine Mn_3O_4 particles are oxidised into Mn_5O_8, whereas oxidation of large particles gives α-Mn_2O_3.[145] Similar effects seem to be expected for other systems.

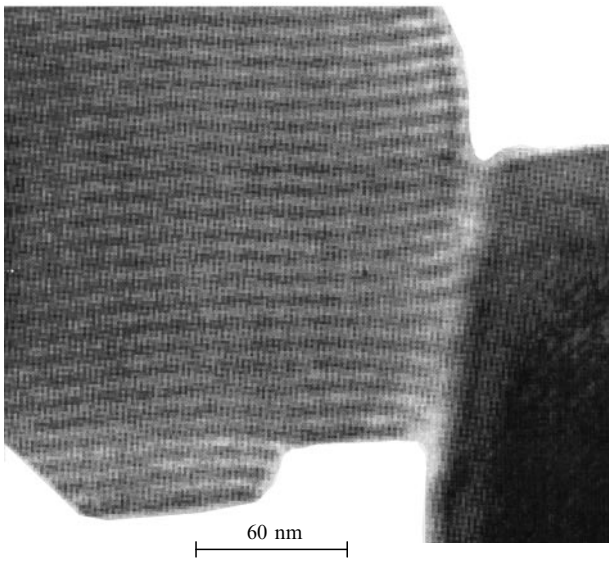


Figure 13. A HREM image of the AgBr–silver stearate interface.[153]

Size effect manifests itself in a somewhat different manner in the chemical and physical development of the latent photographic image, which begins as the Ag particle size exceeds a certain minimum value.[146–148] The usual chemical development involves treatment of silver bromide with a solution of a reducing agent and is due to the catalytic activity of Ag clusters formed upon aggregation of the surface silver atoms and comprising at least five atoms.[149,150] Physical development, or the appearance of an image owing to the deposition of the metal atoms from a solution on the potential crystallisation centres, occurs as the Ag crystallites become larger than the critical size of $\sim$4 nm.

Palladium-free metallisation of dielectrics is similar to physical development and proceeds analogously.[151,152] The process involves deposition of particles on a copper catalyst (obtained by thermal decomposition of copper hypophosphite) from a solution containing the copper salt and a reducing agent. The best results are obtained when the particle size of the copper catalyst is $\sim$25 nm. An increase in the particle size up to 80 nm leads to substantial reduction of the catalytic activity.

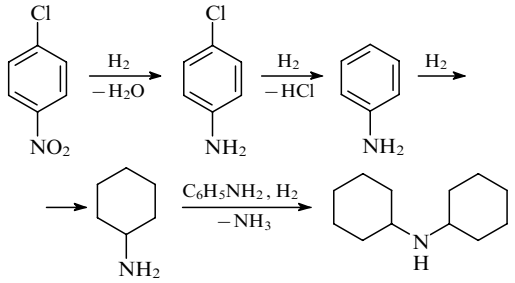
Treatment of silver stearate with bromides results in the formation of nanoscale AgBr particles which serve as sensitisers for silver carboxylates; the latter are candidates for modern photographic processes.[153] The case in point is as follows. Treatment of silver carboxylate with a KBr solution results in the formation of an AgBr particle and leads to the carboxylate lattice distortion at the AgBr–silver carboxylate interface owing to misfit. A HREM image of the AgBr–silver stearate interface is presented in Fig. 13. If the electron beam is oriented parallel to the basal plane of silver stearate, the layers of silver ions form rows of dark bands. As can be seen, these layers are disordered in the interface region and form an interfacial defect zone several nanometres wide. This zone seems to play a significant role in the sensitisation of silver stearate contacting the AgBr particles.

2. Catalytic properties

As mentioned above, the chemical properties of a substance including catalytic ones change on going from a bulk specimen

to a nanocrystal.[34, 154] For instance, the shifts of the energies of the conduction and valence bands in opposite directions cause changes in the photocatalytic properties of semiconductor particles. Khairutdinov[34] has reported numerous examples of the effect of particle sizes on the optical and redox properties as well as on the kinetics of photochemical processes in various oxide and sulfide systems. In particular, it has been shown that the specific photocatalytic activity of TiO_2 depends on its particle size. Unusual chemical properties of α-$Fe_2O_3-SnO_2$ nanocomposites have also been reported.[155] A salient feature of this system obtained by mechanical alloying of a mixture of oxides in high-energy mechanical activators is the high sensitivity and selectivity towards ethanol vapours and a moderate sensitivity to the accompanying gases, CO and CH_4. This is mainly due to the very large area of the contact surface between the two oxides and to the presence of tin ions on the surface of α-Fe_2O_3 particles. As a result, the oxide α-Fe_2O_3, initially assumed to be insensitive to ethanol vapours, acquires sensitivity and a gas sensor based on it allows detection of 1000 ppm of ethanol vapour in air.

A correlation was found between the particle size of a platinum catalyst and its catalytic activity in the reaction of hydrogenation of *p*-chloronitrobenzene, which is often used as a test for catalytic activity in hydrogenation reactions.[156] Using commercial catalysts, the process can proceed up to the stage of formation of chloroaniline. The use of nanoscale platinum particles with sizes 3–4 nm allows the hydrogenation to reach deeper stages with the formation of aniline and cylohexylamine. Nanocrystalline platinum catalyst also appeared to be suitable for further hydrogenation of cylohexylamine to give dicylohexylamine as the end product.



Finally, zinc ferrite nanoparticles were found to exhibit better sorption properties toward H_2S as compared to conventional pure ferrite.[125]

3. Hydrogenation of metal systems

Hydrogenation and dehydrogenation of magnesium have been studied.[157] The use of nanocomposites formed upon mechanical treatment of mixtures of magnesium with nickel and other metals leads to an increase in the rate of hydrogenation and in the yields of the end products. The rate of hydrogen absorption and the hydrogen capacity of the mechanically alloyed composite with stoichiometry Mg_2Ni also increased. Taking $LaNi_5$ as an example, it was shown that the addition of a hydrogenation catalyst (*e.g.*, palladium) to the system together with mechanically treated absorbent leads to even greater increase in the rate of hydrogen intake. Nanocomposites obtained by mechanical treatment of $Fe_{40}Ti_{60}$, $Fe_{50}Ti_{50}$ and $Fe_{67}Ti_{33}$ alloys and by direct mechanochemical alloying of elemental Fe and Ti were found to have a high hydrogen capacity. Compared to the starting alloys, these nanocomposites absorb hydrogen at lower pressures and are stable towards the phase transition of the materials into the γ-phase. Unusual properties of the alloys were explained by the presence of mechanical stress in the crystallites constituting the nanocomposites.

4. Electrochemical and anti-corrosion properties

Electrodes made of mechanically alloyed Ti_2Ni nanocomposite were found to be more efficient in the electrochemical production of hydrogen gas than those produced by conventional procedures.[158]

A distinguishing feature of mechanically alloyed nanomaterials is improved corrosion resistance.[159] Nanostructured material with stoichiometry $Fe_{32}Ni_{36}Cr_{14}P_{12}B_6$ obtained by crystallisation of an amorphous alloy exhibits a higher corrosion resistance than the initial alloy.[160] This was explained by the possibility of fast diffusion of Cr atoms towards the surface along numerous block boundaries in the composite followed by the formation of a protective layer. A similar effect has also been observed.[161] However, it does not always happen that the corrosion resistance increases. In studies of the behaviour of electrochemically deposited Ni–P alloys in 0.1 M H_2SO_4 (see Ref. 162) it was shown that nanocomposites exhibited a reduced corrosion resistance compared to bulk nickel owing to enhanced activities at block boundaries and the possibility of accelerated propagation of the reaction along these boundaries. Nanocomposites with stoichiometry $FeAl_8$ also exhibit a reduced corrosion resistance towards H_2SO_4 and Na_2SO_4 solutions.[163]

Overvoltage (up to 900 mV) on steel cathodes is one of the main sources of energy loss in the electrochemical production of chlorates. It was proposed to use nanocrystalline cathodes prepared by mechanochemical activation of a $RuO_2-Fe-Ti$ mixture.[164] The mechanically alloyed nanocomposite appeared to be an excellent material for cathode production. At a current density of 250 mA cm^{-2} and 70 °C, the overvoltage on the nanocomposite cathodes decreases by 300 mV, which allows a 15% reduction of the expenditure of electrical energy in the production of chlorates. A nanostructured material obtained by mechanical alloying of Ti and TiO in an Ar atmosphere exhibits similar properties.[165] The nanocomposite with oxygen content between 18.5 at.% and 33 at.% can be used as a cathode material in electrochemical production of sodium chlorate. At the operating current density of 250 mA cm^{-2} and solution temperature of 70 °C, the overvoltage on this cathode is 600 mV, which is nearly half as large as the overvoltage on the cathode made of metallic titanium (1107 mV).

5. Size effects in the chemistry of solid organic compounds

Back in the late 1930s, it was found that stearic acid, which usually crystallises in stable β-form, undergoes transformation into the α-form as the crystal size reduces.[166] As the size of molecular crystals decreases, the temperature of the $\alpha-\beta$-transition and the heat of melting also decrease. A change in the ratio between the surface area and volume of molecular crystals leads to changes in both dissolution rate and solubility. Reduction of the size of molecular crystals of chemical compounds used as medicinal drugs to submicron level enhances their biological assimilation and therapeutic efficiency.

Since microscopic and nanoscale molecular crystals are prone to aggregation, it is desirable to place nanoparticles obtained by certain procedures on a support or to prepare nanocomposites of the molecular crystal–support type. One of the well-known and popular methods for the preparation of this sort of nanocomposites involves treatment of the molecular crystal–support mixture in a mechanical activator. This procedure can be conveniently used to prevent transformations of highly active, metastable polymorphous crystalline modifications formed during mechanochemical activation into stable, low activity ones.[167, 168] Here, it is appropriate to refer to a number of studies on the preparation of highly active, readily soluble forms of aspirin, sulfathiazole and other medicinal drugs in order to eliminate their major drawback of low solubility.[169–173]

6. Specific chemical properties of nanocrystals of ionic compounds

Incomplete compensation of the anion and cation charges in ionic compounds leads to the appearance of charged nanoparticles; this is a reason for changes in their chemical properties on going from bulk crystals to nanocrystals.[174] This can be followed taking alkali

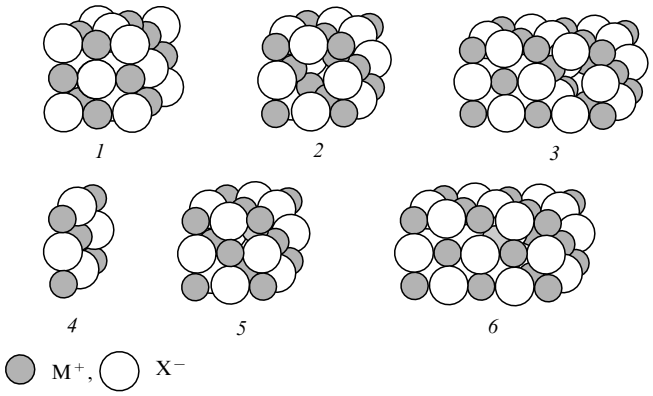


Figure 14. Structures of a (3, 3, 3) nanocrystal of an ionic salt MX (*1*) and clusters that are reactive (*2*, *3*) and passive (*4*–*6*) towards chemisorption of NH_3.
$[M_{14}X_{13}]^+$ (*1*), $[Na_{13}F_{12}]^+$ (*2*), $[Na_{22}F_{21}]^+$ (*3*), $[M_5X_4]^+$ (*4*), $[M_{14}F_{13}]^+$ (*5*) and $[M_{23}X_{22}]^+$ (*6*).[174]

halides as an example. It is known that alkali halide vapours contain charged clusters comprised of, in particular, a small odd number of ions.[175] In larger particles, electroneutrality can also be violated. Figure 14 presents the structure of a cubic nanocrystal of the (3, 3, 3) type (figures denote the number of ions along three edges). As compared to the ideal cubic lattice of ionic salt MX, the nanocrystal lattice is built in such a way that the X^- anions protrude out while the metal cations are recessed.

Charged nanocrystals possess some characteristic properties. For instance, adsorption of polar molecules such as NH_3 and H_2O occurs in different manner depending on the number of lattice sites on the crystal edges. Perfect crystals of the (3, 3, 3) or (3, 3, 5) types do not adsorb polar molecules at room temperature. The loss of two ions (M^+ and X^-, or a single MX unit) leads to the appearance of pits on the surface and to enhancement of the reactivity of crystals. In Fig. 14, the structures of clusters $[M_nX_{n-1}]^+$ (M = Na, X = F) with such pits are shown. These clusters are highly reactive towards NH_3. The structures of $[M_nX_{n-1}]^+$ clusters that are passive towards ammonia are also shown in Fig. 14. It should be mentioned that the cluster structure remains unchanged after the adsorption of a polar molecule.

The reaction of $[Na_{53}F_{52}]^+$ nanoparticles with the surface of silicon occurring in their collisions is yet another example of the reactions of ionic nanoscale clusters. Upon collision, a single fluorine atom is transferred to the silicon surface to form a F–Si bond. The reaction occurs only if the silicon surface is pure. If the silicon surface is preliminarily passivated with hydrogen, the collision event will only result in the cleavage of the nanoparticle.

Condensation of metal atoms on the surface of a nanoparticle leads to the formation of the structures similar to F-centres, where an electron is mainly localised at the anionic vacancy site. These centres are characterised by very low ionisation potentials, *e.g.*, 3 eV for $(Na^+)_n(F^-)_{n-1}e^-$ and 5 eV for $(Cs^+)_{13}(I^-)_{11}e^-$. As the temperature increases, the electron can wander onto the metal cation. A neutral metal atom thus formed leaves the surface. In the case of a perfect nanocrystal without anionic vacancies, an electron that is loosely bound to the surface forms a surface centre, which is a strong electron donor. Photolysis of nanocrystals leads to transfer of the electron from the anion to the cation followed by desorption of a halogen atom from the surface. The transfer energy lies between the energies of analogous transfer in diatomic molecules MX and in bulk $(MX)_\infty$ crystals.

By and large, studies of alkali halide nanocrystals showed that they are more passive towards many reagents as compared to bulk crystals. On the other hand, nanocrystals are prone to self-aggregation; therefore, the search for protective coatings for stabilisation of nanocrystals is topical.

VI. Conclusion

Size effects play an important role in chemical processes including mechanochemical reactions. One should distinguish two groups of size effects. Some of them, inherent in microcrystalline systems, are due to the purely surface phenomena. Stronger phase size effects manifest themselves if the particle size is less than 10 nm. In the former case, the properties of a substance can be interpreted in terms of the classical thermodynamic approach, which includes standard models for taking into account the contribution of surface effects. A basically new situation appears on going to nanoparticles since virtually the whole bulk of the sample under study falls within the action range of surface forces and classification of the atoms into the surface atoms and bulk ones becomes unjustified. In this case, a nanoparticle should be considered to be a cluster or a macromolecule, the structural, thermodynamic and transport properties of which are strongly different from those of the macrocrystal.

Various size effects are observed in heterogeneous systems represented by microcrystalline and nanoscale composites, the properties of which are affected by the interface interaction. Particularly strong are the interface effects typical of heterogeneous systems with the ionic type of bonding. Here, the interface interaction involves the stage of formation of surface defects, which leads to abrupt increase in the ionic conductivity. Similarly to isolated nanoparticles, the material nanocomposites are made of occurs in unusual states and its properties (like those of the adsorption layers) are to a great extent determined by the characteristics of the interface, *i.e.*, by the interatomic interactions within the adjacent phases in the near-surface region.

Practically, nanocomposites represent a promising class of advanced materials with unique electronic properties and high molecular, atomic and ionic mobilities. Mechanochemical processes in heterogeneous mixtures are strongly influenced by size effects, which is of great importance for solving practical tasks associated with controlling the process intensity and obtaining the desired reaction products. Problems which have arisen in this case are directly related to studies of the effect of particle size on the catalytic, electrochemical and specific chemical properties of materials. Therefore, further investigations of size effects in heterogeneous systems are of great theoretical and practical importance.

This review has been written with the financial support of the Programme 'Fundamental Problems of Modern Chemistry. Chemical Transformations Involving Nanoscale and Supramolecular Systems' of the Russian Federation Ministry of Industry, Science and Technology (Grant No. 3) and the US Civilian Research and Development Foundation (Grant REC-008).

References

1. V Boldyrev, M Boulens, B Delmon *The Control of Reactivity of Solids* (Amsterdam: Elsevier, 1979)
2. I D Morokhov, L I Trusov, S P Chizhik *Ul'tradispersnye Metallicheskie Sredy* (Ultradispersed Metallic Media) (Moscow: Atomizdat, 1977)
3. Yu I Petrov *Klastery i Malye Chastitsy* (Clusters and Small Particles) (Moscow: Nauka, 1986)
4. S A Nepiiko *Fizicheskie Svoistva Malykh Metallicheskikh Chastits* (Physical Properties of Small Metallic Particles) (Kiev: Naukova Dumka, 1985)
5. Yu I Vesnin *Vtorichnaya Struktura i Svoistva Kristallov* (Secondary Structure and Properties of Crystals) (Novosibirsk: Institute of Organic and Inorganic Chemistry, Siberian Branch, Russian Academy of Sciences, 1997)
6. L S Palatnik, I I Papirov *Epitaksial'nye Plenki* (Epitaxial Films) (Moscow: Nauka, 1971)
7. Yu F Komnik *Fizika Metallicheskikh Plenok. Razmernye i Strukturnye Effekty* (The Physics of Metallic Films. Size and Structural Effects) (Moscow: Atomizdat, 1979)

8. V G Gryaznov, L I Trusov *Prog. Mater. Sci.* **37** 289 (1993)
9. H Gleiter *Prog. Mater. Sci.* **33** 223 (1989)
10. H Gleiter *J. Appl. Cryst.* **24** 79 (1991)
11. R A Andrievskii, A M Glezer *Fiz. Met. and Metalloved.* **88** 50 (1999) [a]
12. A I Gusev *Usp. Fiz. Nauk* **168** 55 (1988) [b]
13. V L Tauson, M G Abramovich *Fiziko-Khimicheskie Prevrashcheniya Real'nykh Kristallov v Mineral'nykh Sistemakh* (Physicochemical Transformations of Real Crystals in Mineral Systems) (Novosibirsk: Nauka, 1988)
14. A I Rusanov *Solid State Ion.* **75** 275 (1995)
15. A I Rusanov *Zh. Obshch. Khim.* **70** 353 (2000) [c]
16. A I Rusanov *Fazovye Ravnovesiya i Poverkhnostnye Yavleniya* (Phase Equilibria and Surface Effects) (Leningrad: Khimiya, 1967)
17. P Pawlow *Z. Phys. Chem.* **65** 545 (1909)
18. A I Bublik, B Ya Pines *Dokl. Akad. Nauk SSSR* **87** 215 (1952) [d]
19. B Ya Pines *Ocherki o Metallofizike* (Essays on Metallophysics) (Khar'kov: Khar'kov University, 1961)
20. C R M Wronski *Br. J. Appl. Phys., J. Phys. D* **18** 1731 (1967)
21. M Hasegawa, K Hoshino, M Watabe *J. Phys. F., Met. Phys.* **10** 619 (1980)
22. V A Pavlov *Fiz. Met. Metalloved.* **59** 629 (1985) [a]
23. Yu G Sidorov, E M Trukhanov *Poverkhnost'* (6) 106 (1992)
24. I D Morokhov, S P Chizhik, N T Gladkikh, L K Grigor'eva, S V Stepanova *Dokl. Akad. Nauk SSSR* **248** 603 (1979) [d]
25. H Gleiter *Nanostruct. Mater.* **1** 1 (1992)
26. R W Siegel *Phys. New Mater.* **27** 65 (1994)
27. D G Morris *Mechanical Behaviour of Nanostructured Materials* Vol. 2 (Eds M Magini, F H Wohlbier) (Materials Science Foundations Trans. Technology Publications, Zuerich: 1998)
28. G C Benson, T A Claxton *J. Chem. Phys.* **48** 1356 (1968)
29. P W Tasker *Philos. Mag. A Phys. Condens. Matter Defects Mech. Prop.* **39** 119 (1979)
30. N X Sun, K Lu *Phys. Rev. B, Condens. Matter* **54** 6058 (1997)
31. J Friedel *Ann. Phys.* **1** 257 (1976)
32. M R Hoare, P Pal *Adv. Phys.* **20** 161 (1971)
33. A P Alivisatos *Science* **271** 933 (1996)
34. R F Khairutdinov *Usp. Khim.* **67** 125 (1998) [*Russ. Chem. Rev.* **67** 109 (1998)]
35. C L Chien, J Q Xiao, J S Jiang *J. Appl. Phys.* **73** 5309 (1993)
36. D S Lashmore, M P Dariel *J. Electrochem. Soc.* **135** 1221 (1988)
37. S S Parkin, Z C Li, D J Smith *Appl. Phys. Lett.* **58** 2710 (1991)
38. E Yu Ivanov, I G Konstanchuk, B B Bokhonov, V V Boldyrev *React. Solids* **7** 167 (1989)
39. J Eckert, L Schultz, E Hellstern *Appl. Phys. Lett.* **55** 117 (1989)
40. S Ino *J. Phys. Soc. Jpn.* **27** 941 (1969)
41. D J Wales *Science* **271** 925 (1996)
42. T L Hill *Thermodynamics of Small Systems* Part I (New York: Benjamin, 1963)
43. I I Gainutdinov, Yu T Pavlyukhin, V V Boldyrev *Dokl. Akad. Nauk* **344** 189 (1995) [d]
44. I I Gainutdinov, Yu T Pavlyukhin *Dokl. Akad. Nauk* **350** 206 (1996) [d]
45. Ya E Geguzin *Fizika Spekaniya* (The Physics of Caking) (Moscow: Nauka, 1984)
46. B S Bokshtein, Ch V Kopetskii, L S Shvindlerman *Termodinamika i Kinetika Granits Zeren v Metallakh* (Thermodynamics and Kinetics of Grain Boundaries in Metals) (Moscow: Metallurgiya, 1986)
47. J Maier *Ber. Bunsenges. Phys. Chem.* **90** 26 (1986)
48. J Maier *Prog. Solid State Chem.* **23** 171 (1995)
49. V N Chebotin *Fizicheskaya Khimiya Tverdogo Tela* (Physical Chemistry of Solids) (Moscow: Khimiya, 1982)
50. I M Lifshits, A M Kosevich, Ya E Geguzin, in *Poverkhnostnaya Diffuziya i Rastekanie* (Surface Diffusion and Spreading) (Ed. Ya E Geguzin) (Moscow: Nauka, 1969) p. 243
51. Ya I Frenkel' *Kineticheskaya Teoriya Zhidkostei* (Kinetic Theory of Liquids) (Moscow: Academy of Sciences of the USSR, 1945)
52. K L Kliewer, K S Koehler *Phys. Rev. A., At. Mol. Opt. Phys.* **140** 1226 (1965)
53. N F Uvarov, Doctoral Thesis in Chemical Sciences, Institute of Solid State Chemistry and Mechanochemistry, Siberian Branch, Russian Academy of Sciences, Novosibirsk, 1998
54. J Horvath, U Landman *Phys. Rev. Lett.* **82** 3835 (1999)
55. J Horvath, R Birringer, H Gleiter *Solid State Commun.* **62** 319 (1987)
56. B S Bokshtein, G D Breze, P V Kurkin *Izv. Vyssh. Uchebn. Zaved., Chernaya Metallurgiya* **1** 49 (1994)
57. H J Hoffler, R S Averback, H Hahn, H Gleiter *J. Appl. Phys.* **74** 3832 (1993)
58. S M Klotsman *Fiz. Met. Metalloved.* **75** 5 (1993) [a]
59. R E Newnham, D P Skinner, L E Cross *Mater. Res. Bull.* **13** 525 (1978)
60. U Stuhr, H Wipf, T J Udovic, J Weissmueller, H Gleiter *Nanostruct. Mater.* **6** 555 (1995)
61. B Ya Pines, N I Sukhinin *Zh. Tekhn. Fiz.* **26** 2100 (1956) [e]
62. A A Chernov, E I Givargizov, Kh S Bagdasarov, L N Dem'yanets, V A Kuznetsov, A N Lobachev (Eds) *Sovremennaya Kristallografiya* (Modern Crystallography) (Moscow: Nauka, 1980) Vol. 3
63. N F Uvarov, J Maier *Solid State Ion.* **61** 251 (1993)
64. N F Uvarov, V G Ponomareva *Dokl. Aksd. Nauk* **351** 358 (1996) [d]
65. N F Uvarov, E F Hairetdinov, B B Bokhonov, N B Bratel *Solid State Ion.* **86**–**88** (Pt I) 573 (1996)
66. N F Uvarov, B B Bokhonov, V P Isupov, E F Hairetdinov *Solid State Ion.* **74** 15 (1994)
67. N F Uvarov, E F Hairetdinov, I V Skobelev *Solid State Ion.* **86**–**88** 577 (1996)
68. N F Uvarov, I V Skobelev, B B Bokhonov, E F Hairetdinov *J. Mater. Synth. Proc.* **4** 391 (1996)
69. A Adamson *Physical Chemistry of Surfaces* (New York: Wiley, 1974)
70. A D Zimon *Adgeziya Plenok i Pokrytii* (Adhesion of Films and Coatings) (Moscow: Khimiya, 1977)
71. M J Jaycock, G D Parfitt *Chemistry of Interfaces* (New York: Ellis Horwood, 1981)
72. Ya O Bikerman *Usp. Khim.* **41** 1431 (1972) [*Russ. Chem. Rev.* **41** 651 (1972)]
73. A I Rusanov *Dokl. Akad. Nauk SSSR* **261** 700 (1981) [d]
74. J Maier *J. Phys. Chem. Solids* **46** 309 (1985)
75. A K Shukla, R Manoharan, J B Goodenough *Solid State Ion.* **26** 5 (1988)
76. B Zhu, B-E Mellander *Solid State Ion.* **77** 244 (1995)
77. B Zhu *Solid State Ion.* **125** 397 (1999)
78. B Zhu, B-E Mellander *Solid State Ion.* **70** (Pt 1) 285 (1994)
79. Z-Y Zhao, C-Y Wang, S-Y Dai, L-Q Chen *Solid State Ion.* **9**/**10** 1175 (1983)
80. Yu Ya Gurevich *Dokl. Akad. Nauk SSSR* **222** 143 (1975) [d]
81. J B Boyce, B A Huberman *Phys. Rep.* **51** 190 (1979)
82. N G Hainovsky, J Maier *Phys. Rev. B, Condens. Matter* **51** 15789 (1995)
83. V N Bondarev, A B Kuklov *Elektrokhimiya* **26** 1397 (1990) [f]
84. N F Uvarov, E F Hairetdinov *J. Solid State Chem.* **62** 3 (1985)
85. N F Uvarov, V P Isupov, V Sharma, A K Shukla *Solid State Ion.* **51** 41 (1992)
86. V M Kosevich, V M Ievlev, L S Palatnik, A I Fedorenko *Struktura Mezhkristallitnykh i Mezhfaznykh Granits* (Structure of Crystallite and Phase Boundaries) (Moscow: Metallurgiya, 1980)
87. L S Palatnik, M Ya Fuks, V M Kosevich *Mekhanizm Obrazovaniya i Substruktura Kondensirovannykh Plenok* (The Mechanism of Formation and Substructure of Condensed Films) (Moscow: Nauka, 1972)
88. W A Jesser, D Kulmann-Wilsdorf *Phys. Status Solidi B* **19** 95 (1967)
89. V A Gusev, V A Gagarina, E M Moroz, E A Levitskii *Kinet. Katal.* **17** 500 (1976) [g]
90. N F Uvarov, M C R Shastry, K J Rao *Rev. Solid State Sci.* **4** 61 (1990)
91. E F Hairetdinov, N F Uvarov *Mater. Sci. Forum* **88**–**90** 723 (1992)
92. N F Uvarov, E F Khairetdinov, N B Bratel' *Elektrokhimiya* **29** 1406 (1993) [f]
93. N F Uvarov, P Vanek, M Savinov, V Zelezny, J Studnicka, J Petzelt *Solid State Ion.* **127** 253 (2000)
94. N F Uvarov, A A Politov, in *Abstracts of Reports of the 12th International Conference on Solid State Ionics, Thessaloniki, 1999* M-06-P
95. N F Uvarov, P Vanek, Yu I Yuzyuk, V Zelezny, J Studnicka, B B Bokhonov, V E Dulepov, J Petzelt *Solid State Ion.* **90** 201 (1996)
96. V G Ponomareva, N F Uvarov, G V Lavrova, E F Hairetdinov *Solid State Ion.* **90** 161 (1996)
97. V G Ponomareva, G V Lavrova, L G Simonova *Solid State Ion.* **118** 317 (1999)
98. N F Uvarov, L I Brezhneva, E F Hairetdinov *Solid State Ion.* **136**–**138** 1273 (2000)

99. P Chowdary, V B Tare, J B Wagner *J. Electrochem. Soc.* **132** 123 (1985)
100. A C Khandkhar, J B Wagner *Solid State Ion.* **20** 267 (1986)
101. C A Angell, D B Helphrey *J. Phys. Chem.* **75** 2306 (1971)
102. A Kumar, K Shahi *Solid State Ion.* **68** 71 (1994)
103. G Heinike *Tribochemistry* (Berlin: Akademie-Verlag, 1984)
104. V V Boldyrev *Eksperimental'nye Metody v Mekhanokhimii Tverdykh Neorganicheskikh Veshchestv* (Experimental Methods in Mechanochemistry of Solid Inorganic Substances) (Novosibirsk: Nauka, 1983)
105. C C Koch *Annu. Rev. Mater. Sci.* **19** 121 (1989)
106. E G Avvakumov *Mekhanicheskie Metody Aktivatsii Khimicheskikh Protsessov* (Mechanical Methods of Activation of Chemical Processes) (Novosibirsk: Nauka, 1986)
107. *Mekhanokhimicheskii Sintez v Neorganicheskoi Khimii* (Mechanochemical Synthesis in Inorganic Chemistry) (Novosibirsk: Nauka, 1991)
108. *Proceedings of the 1st International Symposium on Mechanical Alloying, Kyoto, 1991*
109. P Yu Butyagin *Usp. Khim.* **63** 1031 (1994) [*Russ. Chem. Rev.* **63** 965 (1994)]
110. E Gaffet, M Abdellaoui, N N Malhourux-Gaffet *Mater. Trans. JIM* **36** 198 (1995)
111. M Dadras, D S Morris *Scr. Metall. Mater.* **28** 1245 (1993)
112. T Itsukaichi, M Umemoto, J G Cabanas-Moreno *Scr. Metall. Mater.* **29** 583 (1993)
113. E Ivanov, K Sumiyamann, H Yamauchi, K Jamai, K Suzuki *J. Alloys Compd.* **198** 195 (1993)
114. P Matteazzi, G Le Caer, A Mocellin *Ceram. Int.* **23** 39 (1997)
115. K B Gerasimov, S V Pavlov, S V Mytnichenko, V A Chernov, S G Nikitenko *J. Alloys Compd.* **252** 179 (1997)
116. M A Uimin, A Ye Yermakov, V V Serikov, A Yu Korobeinikov, A K Shtolz *Phys. Status Solidi A* **165** 337 (1998)
117. V A Ivchenko, M A Uimin, A Ye Yermakov, A Yu Korobeinikov *Surf. Sci.* **440** 420 (1999)
118. A V Demenko, A I Maslii, V V Boldyrev *J. Mater. Synth. Proc.* **3** 303 (1995)
119. A R Yavary, O Dabrohlav *Mater. Sci. Forum* **225–227** 295 (1996)
120. M L Trudeau, R Schulz, D Dussault, A Van Neste *Phys. Rev. Lett.* **64** 99 (1990)
121. R Schulz, M Simoneau, J Lantegne *Physica C* **233** 113 (1994)
122. R Schulz, M L Trudeau, D Dussault, A Van Neste, L Dignard-Bailey *Mater. Sci. Eng. A, Struct. Mater.* **179** 516 (1994)
123. P Matteazzi, G LeCaer *J. Am. Ceram. Soc.* **74** 1382 (1991)
124. P Matteazzi, G LeCaer *Proc. Adv. Mater. 1* **135** 20 (1991)
125. P Matteazzi, G LeCaer *J. Alloys Compd.* **187** 305 (1992)
126. A Ye Yermakov, N V Mushnikov, M A Uimin, N K Zajkov, A Yu Korobeinikov, A K Shtolz, V V Serikov *Mater. Sci. Forum* **269–272** 907 (1998)
127. G Nicoara, D Fratiloiu, M Nogues, J L Dormann, F Vasiliu *Mater. Sci. Forum* **235–238** 145 (1997)
128. P G McCormick, in *Handbook on the Physics and Chemistry of Rare Earth* Vol. 24 (Amsterdam: Elsevier, 1997) p. 47
129. T Tsuzuki, W T A Harrison, P G McCormick *J. Alloys Compd.* **281** 146 (1998)
130. T Tsuzuki, J Ding, P G MacCormick *Physika B* **239** 378 (1997)
131. T F Grigorjeva, A P Barinova, G N Kryukova, V V Boldyrev, in *Proceedings of the 5th European Conference on Advanced Materials, Processes and Applications, Dodrecht, 1997* Vol. 2, p. 333
132. V Sepelak, A Yu Rogachev, U Steinike, D-Chr Uecker, F Krumeich, S Wissman, K D Becker *Mater. Sci. Forum* **235–238** 139 (1997)
133. B B Bokhonov, I G Konstanchuk, V V Boldyrev *Mater. Res. Bull.* **30** 1277 (1995)
134. A P Nemudry *React. Solids* **3** 317 (1987)
135. A V Besserguenev, A M Fogg, R J Francis, S J Price, D O'Hare, V P Isupov, B P Tolochko *Chem. Mater.* **9** 241 (1997)
136. V P Isupov, Doctoral Thesis in Chemical Sciences, Institute of Solid State Chemistry and Mechanochemistry, Siberian Branch, Russian Academy of Sciences, Novosibirsk, 1998
137. V Rives, M A Ulibarri *Coord. Chem. Rev.* **181** 61 (1999)
138. V P Isupov, L E Chupakhina, R P Mitrofanova, K A Tarasov *Zh. Strukt. Khim.* **39** 453 (1998) [h]
139. E I Bakchinova, V P Isupov, V A Poluboyarov, V V Boldyrev *Dokl. Akad. Nauk* **324** 592 (1992) [d]
140. V P Isupov, K A Tarasov, L E Chupakhina *Dokl. Akad. Nauk* **324** 1217 (1992) [d]
141. V V Boldyrev, E V Boldyreva *Mater. Sci. Forum* **88–90** 711 (1992)
142. E V Boldyreva *J. Therm. Anal.* **38** 89 (1992)
143. W Feitknecht *Pure Appl. Chem.* **9** 423 (1964)
144. B Gillot, A Rousset, G Dupre *J. Solid State Chem.* **25** 263 (1978)
145. B Gillot, J Tyranowic, A Rousset *Mater. Res. Bull.* **10** 775 (1975)
146. H Reinder, L Hamburger *Recl. Trav. Chim. Pays-Bas* **50** 475 (1931)
147. E A Galashin *Dokl. Akad. Nauk SSSR* **184** 639 (1969) [d]
148. C E Mees, T H James *The Theory of Photographic Process* (New York: Macmillan, 1966)
149. J F Hamilton, P C Logel *Photogr. Sci. Eng.* **18** 507 (1974)
150. J W Mitchell *J. Imaging Sci. Technol.* **38** 193 (1995)
151. O I Lomovskii, Doctoral Thesis in Chemical Sciences, Institute of Solid State Chemistry and Mechanochemistry, Siberian Branch, Academy of Sciences of the USSR, Novosibirsk, 1990
152. A Ya Lushnikov, O I Lomovskii *Izv. Sib. Otd. Akad. Nauk SSSR, Ser. Khim. Nauk* (2) 18 (1989)
153. B B Bokhonov, L P Burleva, W C Frank, J R Miller, M R V Sahyun, D R Whitcomb, J M Winslow, C Zou *J. Imaging Sci. Technol.* **40** 85 (1996)
154. J F Hamilton *J. Vac. Sci. Technol.* **13** 319 (1976)
155. J Z Jiang, R Lin, W Lin, K Nielsen, S Morup, K Dam-Johansen, R Clasen *J. Phys. D Appl. Phys.* **30** 1459 (1997)
156. G Vitulli, E Pitzalis, A Verrazani, P Pertici, P Salvadori, G Marta *Mater. Sci. Forum* **235–238** 929 (1997)
157. I G Konstanchuk, E Yu Ivanov, V V Boldyrev *Usp. Khim.* **67** 75 (1998) [*Russ. Chem. Rev.* **67** 69 (1998)]
158. T Benameur, B Rezgui, A R Yavary, R Durand *Mater. Sci. Forum* **235–238** 917 (1997)
159. E M Gutman *Mekhanokhimiya i Zashchita Metallov ot Korrozii* (Mechanochemistry and Protection of Metals from Corrosion) (Moscow: Metallurgizdat, 1981)
160. S J Trope, B Ramaswami, K T Aust *J. Electrochem. Soc.* **135** 2162 (1988)
161. O El Kedim, M Tachikart, E Gaffet *Mater. Sci. Forum* **225–227** 825 (1996)
162. R Rofagha, R Langer, A M El-Sherik, U Erb, G Palumbo, K T Aust *Scr. Metall. Mater.* **25** 2867 (1991)
163. M Schneider, W Zeiger, D Scharnweber, H Worch *Mater. Sci. Forum* **225–227** 819 (1996)
164. A Van Neste, S H Yip, S Jin, S Boily, E Ghali, D Guay, R Schulz *Mater. Sci. Forum* **225–227** 795 (1996)
165. E Tremblay, O Savadogo, S Boily, A Van Neste, R Schulz *Mater. Sci. Forum* **225–227** 813 (1996)
166. P A Thiessen *Angew. Chem.* **51** 318 (1938)
167. A Ikekawa, S Hoyakawa *Bull. Chem. Soc. Jpn.* **54** 2587 (1981)
168. A M Dubinskaya *Khim.-Farm. Zh.* **23** 755 (1989)
169. T Shakhtshneider, V V Boldyrev, in *Reactivity of Molecular Solids* (Eds E Boldyreva, V V Boldyrev) (Chichester: Wiley, 1999) p. 271
170. A V Dushkin, Z U Rykova, T P Shakhtshneider, V V Boldyrev *Int. J. Mechanochem. Mech. Alloying* **1** 48 (1994)
171. A Yu Yagodin, A V Dushkin, V V Boldyrev *Pharmazie* **3** 69 (1991)
172. V V Boldyrev, T P Shahtshneider, L P Burleva, V A Severzev *Drug Develop. Industr. Pharm.* **20** 1103 (1994)
173. T P Shakhtshneider, M A Vasilchenko, A A Politov, V V Boldyrev *Int. J. Pharm.* **130** 25 (1996)
174. R L Whetten *Acc. Chem. Res.* **26** 49 (1993)
175. P Davidovits, D L McFadden (Eds) *Alkali Halide Vapours* (New York: Academic Press, 1979)

[a] — *Phys. Met. Metallogr. (Engl. Transl.)*
[b] — *Physics-Uspekhi (Engl. Transl.)*
[c] — *Russ. J. Gen. Chem. (Engl. Transl.)*
[d] — *Dokl. Chem. Technol., Dokl. Chem. (Engl. Transl.)*
[e] — *Tech. Phys. (Engl. Transl.)*
[f] — *Russ. J. Electrochem. (Engl. Transl.)*
[g] — *Kinet. Catal. (Engl. Transl.)*
[h] — *Russ. J. Struct. Chem. (Engl. Transl.)*
[i] — *Chem. Pharm. J. (Engl. Transl.)*